8

Plumes and their deposits

Paul E. Geissler and David B. Goldstein

8.1 INTRODUCTION

The *Voyager 1* spacecraft's discovery in 1979 of enormous plumes of dust and gas reaching hundreds of kilometers above Io's surface provided the first spectacular evidence of active volcanism beyond Earth. Four months later, the fly-by of *Voyager 2* revealed changes in the distribution and vigor of the plumes that hinted at the variability of explosive eruptions on Io. Decades of observations by ground-based and Earth-orbiting telescopes and the recent targeted campaigns by the *Galileo* and *Cassini* missions have since revealed much about the nature of Io's volcanic plumes. At the same time, theoretical advances have deepened our understanding of the dynamics and chemistry of these intriguing phenomena.

Over 400 volcanic paterae dot the surface of Io (Radebaugh *et al.*, 2001), and more than 150 active hot spots have been detected through their thermal emission (Lopes *et al.*, 2004). Only a handful of these volcanoes have so far been seen to produce explosive eruptions (defined here as emplacing pyroclastic deposits). Plumes of gas and dust have been observed from 16 different volcanic centers on Io (Table 8.1). Several other sites of recent plume activity can be inferred from surface changes and frost deposits. The temporal behavior of the plumes ranges from episodic big bangs to quasi-continuous fountains; several of the plumes have apparently been sustained for decades. Observations of the plumes and their deposits indicate two distinct classes of plumes on Io: giant plumes that vent sulfur-rich gases from the interior of the moon and spray-paint the surface with enormous red rings, and more numerous smaller plumes that are produced when hot flows of silicate lava impinge on volatile surface ices of SO_2.

Io's plumes are generated when volatile vapors are violently expelled from volcanoes, at speeds reaching up to $1\,km\,s^{-1}$. Many of the dynamical features displayed by Io's plumes are expected from the flow of gas out of a nozzle and into a near-vacuum. Close to the vent, the gas behaves as a continuum and the

Table 8.1. Plumes observed on Io. Latitudes and longitudes are those of the center of the surface changes produced by the plumes. Heights of dust columns are listed for *Galileo* era plumes seen near the limb, corrected for geometric foreshortening.

Name	Lat.	Lon.	Orb.	Image	Filter	GMT (M/D/Y H:M)	Res. (km/pixel)	Meas. height (km)	Meas. error (km)	Corr. height (km)	Corr error (km)	Position/ notes
Kanehekili	−19	34	G8	s0394435001	VIOLET	5/6/1997 22:52	13.0	70.2	13	75	14	limb
	−16	36	E11	s0420900323	VIOLET	11/8/1997 18:45	19.5	100.7	20	101	20	limb
Masubi	−44	54	C21	s0506406118	VIOLET	7/2/1999 4:04	2.6	82.2	20	87	21	limb
	−44	54	C21	s0506406153	VIOLET	7/2/1999 4:05	3.3	91.0	10	96	11	limb
	−44	54	C21	s0506406800	GREEN	7/2/1999 4:11	1.6	74.9	10	80	11	limb
	−44	54	C21	s0506584123	VIOLET	7/3/1999 10:04	16.7	93.9	20	99	21	limb
	−44	54	C22	s0512352501	VIOLET	8/12/1999 22:09	10.8	63.1	20	64	20	limb
	−44	54	C22	s0512375600	VIOLET	8/13/1999 2:02	12.8	64.0	20	92	29	limb
	−44	54	I31	s0615693301	VIOLET	8/7/2001 12:58	19.6	61.4	20	91	30	limb
	−44	54	I31	s0615816301	VIOLET	8/8/2001 9:42	19.9					terminator
Amirani	21	112	C22	s0512420523	VIOLET	8/13/1999 9:37	15.9	36.6	15	66	27	limb
	21	112	C22	s0512436201	GREEN	8/13/1999 12:15	16.4	72.9	15	75	15	limb
	21	112	C22	s0512436223	VIOLET	8/13/1999 12:15	16.4	73.6	15	76	15	limb
	21	112	C22	s0512447700	GREEN	8/13/1999 14:11	16.5	36.4	20	86	47	limb
	21	112	C22	s0512447723	VIOLET	8/13/1999 14:12	16.5	36.8	20	87	47	limb
	23	115	E4	s0374850023	VIOLET	12/20/1996 10:27	18.3	40.4	20	72	36	limb
	24	116	G8	s0394478123	VIOLET	5/7/1997 6:09	9.8	52.8	15	60	17	limb
Maui	19	122								57–148		VGR obs.
												Cassini obs.
Tvashtar	63	122	G29									
Thor	39	131	I31	s0615325146	VIOLET	8/4/2001 22:56	18.3	103.3	18	107	19	limb
Prometheus	−1	155	G2	s0359402500	VIOLET	9/2/1996 23:15	30.8					terminator
	−1	155	G2	s0359653300	VIOLET	9/4/1996 17:31	21.9					terminator
	−1	155	G2	s0359722942	VIOLET	9/5/1996 5:15	18.7	56.5	20	86	30	limb
	−1	155	G2	s0359729642	VIOLET	9/5/1996 6:23	19.0	76.1	20	76	20	limb
	−1	155	G2	s0359736542	VIOLET	9/5/1996 7:33	19.3	38.9	20	67	35	limb
	−1	155	C3	s0368558239	CLEAR	11/6/1996 6:10	3.5					disk
	−1	155	E4	s0374575922	VIOLET	12/19/1996 12:15	11.7					disk
	−1	155	E6	s0383600826	VIOLET	2/19/1997 21:07	10.9					terminator
	−1	155	G8	s0394435001	VIOLET	5/6/1997 22:52	13.0					terminator
	−1	155	G8	s0394505123	VIOLET	5/7/1997 10:41	10.0	89.9	10	90	10	limb
	−1	155	C9	s0401785407	VIOLET	6/27/1997 13:33	8.3	66.4	16	71	17	limb

				s0401863204	VIOLET	6/28/1997 2:40	6.2	295.7	60	74	15	disk
	−1	155	C9	s0401876300	VIOLET	6/28/1997 4:52	12.7					terminator
	−1	155	E11	s0420730085	VIOLET	11/7/1997 14:05	9.3	68.2	10	79	12	limb
	−1	155	E11	s0420789285	VIOLET	11/8/1997 0:03	8.0					terminator
	−1	155	C21	s0506492200	VIOLET	7/2/1999 18:34	10.0					terminator
	−1	155	C22	s0512466924	VIOLET	8/13/1999 17:26	16.3	48.9	20	72	29	limb
Culann	−20	161	G1	s0350029700	CLEAR	6/30/1996 3:46	10.5					eclipse
	−20	161	G2	s0359729642	VIOLET	9/5/1996 6:23	19.0					limb, marginal detection
	−20	161	G8	s0394394200	CLEAR	5/6/1997 16:00	18.6					eclipse
	−20	161	E15	s0449843800	CLEAR	5/31/1998 0:17	14.0					eclipse
	−20	161	E15	s0449847913	CLEAR	5/31/1998 0:58	13.4					eclipse
Zamama	18	171	G1	s0349673978	VIOLET	6/26/1996 15:49	13.9	75.3	15	79	16	limb
	18	172	G8	s0394519124	VIOLET	5/7/1997 13:03	10.5	61.0	20	62	20	limb
	19	175	E11	s0420730085	VIOLET	11/7/1997 14:05	9.3	29.6	10	80	27	limb
	19	175	E11	s0420743485	VIOLET	11/7/1997 16:20	9.0	66.1	20	67	20	limb
	19	175	E11	s0420789285	VIOLET	11/8/1997 0:03	8.0					disk
	18	176	E14	s0440873652	VIOLET	3/29/1998 0:37	3.0					disk
	18	176	I24	s0520873452	VIOLET	10/11/1999 18:05	6.7					terminator
Volund	22	177								96–98		VGR obs.
Marduk	−23	211	G8	s0394552545	VIOLET	5/7/1997 18:41	11.4	51.0	20	52	20	limb
	−23	211	E11	s0420773085	VIOLET	11/7/1997 21:19	8.2	76.0	8	76	8	limb
	−25	212	C21	s0506405768	VIOLET	7/2/1999 4:01	2.9	32.9	10	92	28	limb
Pillan	−11	242	C9	s0401863204	VIOLET	6/28/1997 2:40	6.2	99.3	20	109	22	limb
	−12	243	E11	s0420789285	VIOLET	11/8/1997 0:03	8.0	105.4	25	118	28	limb
Pele	−18	255	E4	s0374850023	VIOLET	12/20/1996 10:27	18.3	180.9	20	426	47	limb
Loki	17	301								16–35		VGR obs.
	19	305								166–382		VGR obs.
Ra	−10	323	G1	s0350024288	VIOLET	6/29/1996 2:50	9.9	91.8	10	104	11	limb
Acala	10	335	G7	s0389608268	CLEAR	4/3/1997 1:29	33.3					eclipse
	10	335	G8	s0394394200	CLEAR	5/6/1997 16:00	18.6					eclipse
	10	335	C9	s0401957745	CLEAR	6/28/1997	14.6					eclipse
	10	335	C10	s0413546765	CLEAR	9/18/1997 3:34	13.3					eclipse
	10	335	C10	s0413799045	CLEAR	9/19/1997 22:40	11.4					eclipse
	10	335	E11	s0420858600	CLEAR	11/8/1997 11:44	13.7					eclipse
	12	331	E15	s0449843800	CLEAR	5/31/1998 0:17	14.0					eclipse
	12	331	E15	s0449847913	CLEAR	5/31/1998 0:58	13.4					eclipse

flow is dominated by momentum. The gas quickly accelerates and cools, both due to expansion and to thermal radiation. At the top of the plume, momentum is overcome by gravity and the gas collapses back toward the surface. Depending on plume density, the high-altitude flow may produce a canopy shaped shock as it encounters downfalling gas and decelerates below the speed of sound. The falling gas, approaching the top of the day-time atmosphere, may experience a second shock as it deposits a ring of condensed material about the source region. Moderately energetic flows can bounce when they re-impact, scouring the surface and producing successive concentric rings. Very small particles of solid or liquid phases will flow with the gas, but larger dust particles will decouple from the flow and follow ballistic trajectories.

In addition to presenting a fascinating display of gas dynamics, Io's plumes are important because of their effects on the surface and atmosphere of the satellite. Io's surface is continually coated with the fallout from plumes in a constantly changing variety of colors. Plumes contribute to the rapid resurfacing responsible for the burial of impact craters on the satellite's young surface. Explosive eruptions demonstrate the diverse styles of volcanic activity and provide direct indications of the composition of Io's interior. The plumes also add substantially to the structure of the tenuous atmosphere, affecting the composition and flux of materials escaping from Io and feeding the neutral clouds and plasma torus. Ejection of dust from Io's largest plumes creates the dust streams that emanate from Io and pervade the Jovian system and interplanetary space far from Jupiter.

This chapter will review what has so far been learned about Io's volcanic plumes from Earth-based observations, theoretical and numerical studies, and the recent results of *Galileo* and *Cassini*, and will highlight some of the outstanding unanswered questions. Io's plumes were vigorously studied soon after their discovery, and many important papers were published prior to the arrival of *Galileo* with results that remain useful today. Cook *et al.* (1979) first considered both ballistic and hydrodynamic models as limiting cases of plume flow, and concluded that the plume characteristics were best explained by dense flows that produced canopy shocks. Strom and Schneider (1982) presented detailed observational descriptions of the plumes that were imaged by *Voyagers 1* and *2*. Kieffer (1982) provided a thorough theoretical treatment of the thermodynamics of plumes and their possible sources. Johnson and Soderblom (1982) pointed out the possible roles of plumes in global resurfacing and heat flow. McEwen and Soderblom (1983) first recognized the distinction between the two classes of plumes on Io that is a central theme of this chapter.

Compared with the sources and sinks of plume materials, the appearance and behavior of Io's plumes are fairly well known from direct observation. Much of the uncertainty concerning these phenomena comes from considering the volcanic sources of plumes and the ultimate fate of plume materials long after they are shot from the surface. The nature of the vents and the volcanic plumbing that produces plumes is touched upon in Chapter 7. The influence of plumes on the structure and composition of the atmosphere is covered in Chapter 10. The escape of materials from Io and the effects of volcanism on the neutral clouds, plasma torus, and Jovian magnetosphere are described in Chapter 11.

8.2 OBSERVATIONS OF PLUMES

The plumes of Io have been studied with a variety of observational approaches. During day-time, plumes can best be seen when illuminated at high phase angles, via sunlight reflected by fine particles of solid or liquid that are entrained with or condensed from the vapor. Plumes have also been imaged in transmitted light, silhouetted against the disk of Jupiter (Spencer *et al.*, 1997) or casting shadows on the surface of Io. Plume gases have been observed through auroral emissions at near-infrared (de Pater *et al.*, 2002), visible (Geissler *et al.*, 1999, 2004a), and ultraviolet (Roesler *et al.*, 1999; Retherford *et al.*, 2000) wavelengths and inferred from analyses of thermal emission at millimeter wavelengths (Lellouch *et al.*, 1992, 1996). These diverse data sets yield various perspectives of plumes that are the pieces of a puzzle that must be put together by theory.

8.2.1 Dust

The most detailed information on plume morphologies comes from close-up images of eruptions that were taken in sunlight and show the distribution of dust-sized particles which may include entrained silicates, snow, and supercooled droplets. Consistent with the evidence presented by plume deposits and surface changes, images of these dust columns suggest two distinct types of volcanic plumes on Io.

Most dust plumes tend to be small and optically dense, typically reaching heights of less than 100 km. The archetype of this class of smaller plumes is Prometheus (Figure 8.1), which has been seen actively fountaining SO_2-rich gas and dust at every favorable observing opportunity since the *Voyager* fly-bys. The location of Prometheus's source has migrated more than 80 km over the 20 year interval between *Voyager* and *Galileo*, tracking the foot of a lava flow that has been issuing from a small patera to the east (McEwen *et al.*, 1998). The presently active plume is centered over an expanse of recently emplaced silicate lava. It is suggested that the plume arises when hot silicate lavas bury the icy, SO_2-rich substrate (Kieffer *et al.*, 2000). Smaller jets at the active margin of the flow can also be seen in *Galileo* images (Milazzo *et al.*, 2001). Several similarly sized plumes are associated with lava flows elsewhere on the satellite. The morphology of these smaller plumes ranges from fountain- to umbrella-shaped, with an optically thick core near the source region. An image of the shadow of Prometheus, taken during *Galileo*'s orbit 9, shows a dense vertical column of dust topped by a mushroom-shaped canopy. A central spike in the column may be populated by fine particulates (Zhang *et al.*, 2004). Wispy filaments have been spotted in the dust streams from Prometheus, suggestive of plume electrification (Peratt and Dessler, 1988).

The second class of plumes, exemplified by Pele (Figure 8.2), is rarer and more energetic than the first. These giant plumes are faint and difficult to see in reflected light, but typically form shield-shaped dust streams that reach heights up to 400 km. Pele was nearly invisible to *Galileo*'s imaging system but could be clearly seen spanning an expanse more than 1,000 km across in ultraviolet images taken by *Cassini*'s camera (Porco *et al.*, 2003). Pele's source appears to be an actively

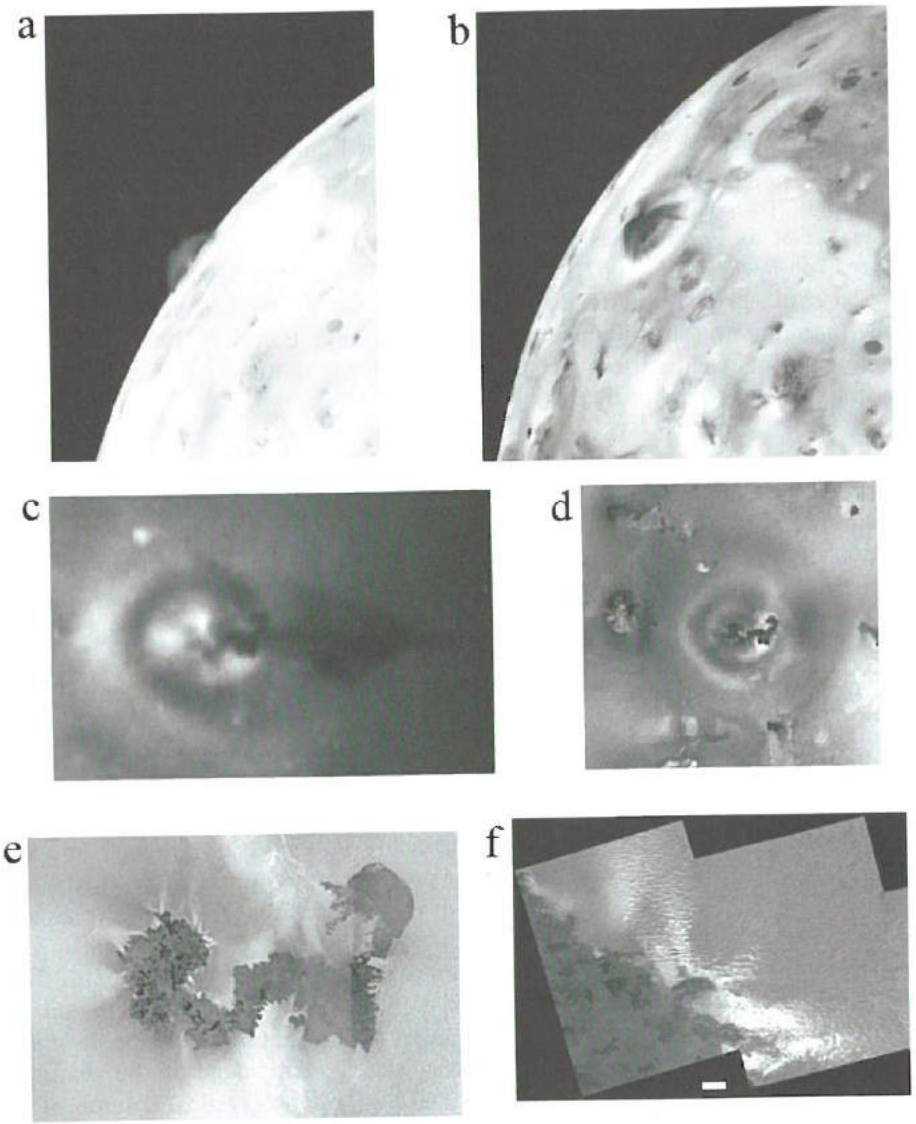

Figure 8.1. Prometheus, the archetype of small plumes. (a) *Voyager 1* image profiling Prometheus's umbrella-shaped dust plume along Io's limb (NASA press release image PIA00374). (b) Oblique *Voyager 1* image showing filaments in the dust plume (NASA press release image PIA00373). (c) *Galileo* image of the shadow cast by the plume (NASA press release image PIA00703). (d) *Galileo* violet-filter image of Prometheus's concentric rings, taken on orbit 14 (NASA press release image PIA01604). (e) *Galileo* image of the source of the plume, a lava flow that extends ~100 km westwards from Prometheus Patera (NASA press release image PIA2565). (f) Close-up view of the margin of the lava flow, showing fresh deposits of bright SO_2 frost where the dark silicate lava has encroached on the icy surface. Scale bar is 1 km long (NASA press release image PIA02568).

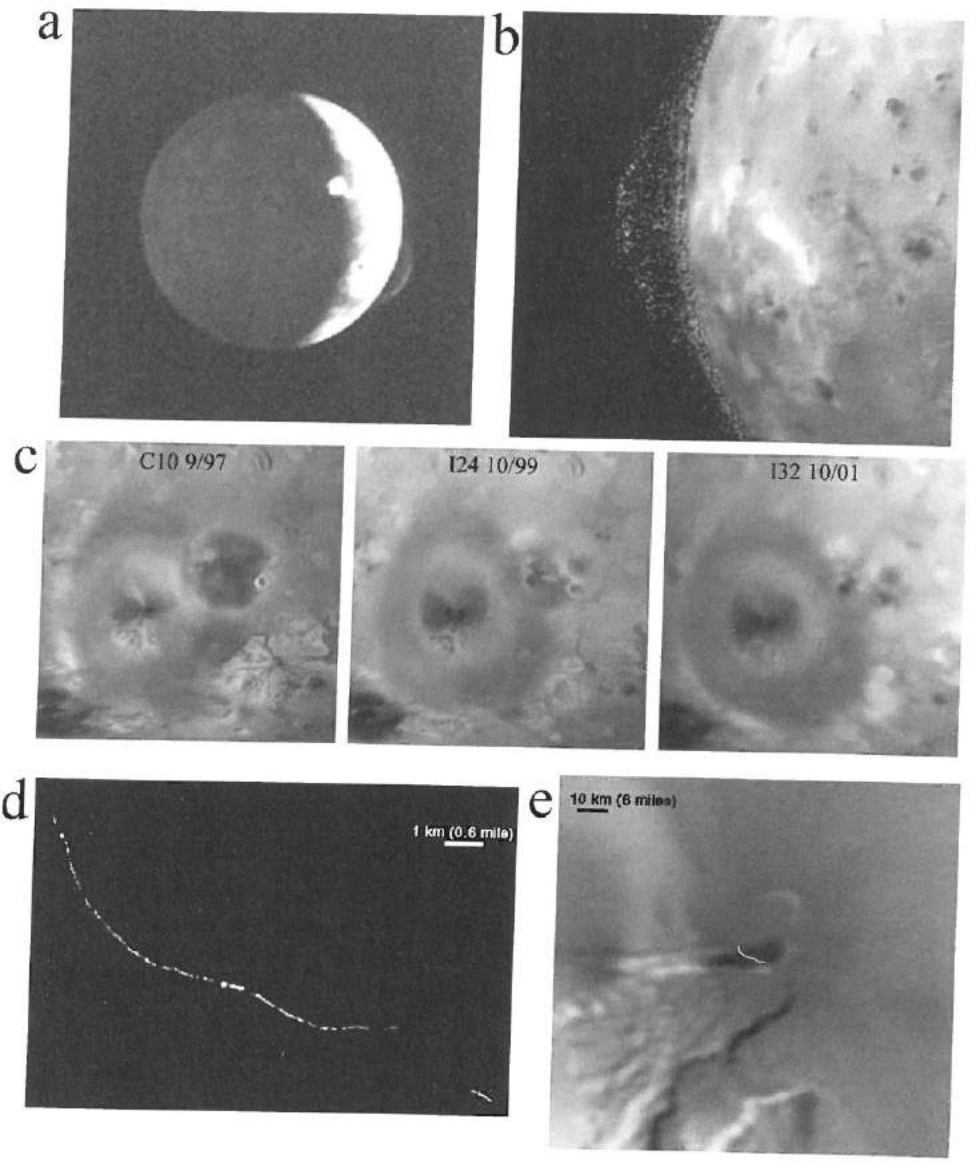

Figure 8.2. Pele, the archetype of giant plumes. (a) Discovery image: this low-resolution *Voyager 1* optical navigation image provided the first spectacular evidence of active extra-terrestrial volcanism. Pele is on the sunlit limb, Loki is on the terminator (NASA press release image PIA00379). (b) *Voyager 1* ultraviolet image of the dust plume (NASA press release image PIA01530). (c) *Galileo* images showing changes in Pele's plume deposit over a 4-year period. (d) Hot lava at the source of the plume glows in the darkness of Io's night (NASA press release image PIA02511). (e) The night-time image placed in the context of a *Voyager 1* image, showing that the glows occur along the edge of the patera, similar to terrestrial lava lakes (NASA press release image PIA02511).

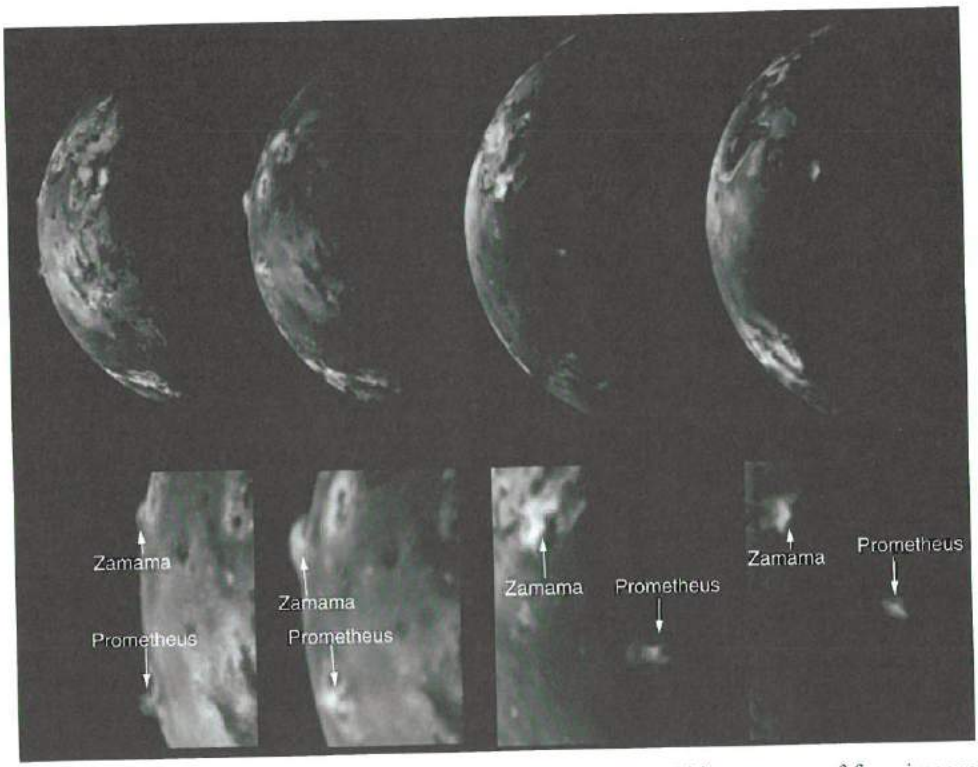

Figure 8.3. Zamama and Prometheus (see also color section). This sequence of four images watches as two small plumes rotate onto the disk of Io. The blue colors of the plumes are caused by the light-scattering properties of the dust particles (NASA press release image PIA01652).

overturning lava lake that continually exposes hot lava and exhales sulfur-rich gases from Io's interior.

Dust plumes can be seen in daylight to have bluish colors that contrast with the yellow and orange hues of Io's surface (Figure 8.3). The blue colors are caused by the wavelength-dependent light-scattering behavior of small dust particles. The color, brightness and opacity of dust plumes yield information on the dust grain size distributions and the dust deposition rates of the eruptions. However, the dust particle sizes and dust plume masses derived from photometric analyses vary greatly, depending on the assumptions made.

Collins (1981) applied a Rayleigh scattering law to *Voyager 1* color observations of Loki's plume, effectively assuming that the particles were much smaller than the wavelength of visible light. He found that particles on the order of 1–10 nm in radius comprised most of the mass of the plume. A second population of particles with distinctly redder colors was found in the core of the plume and interpreted to be made up of particles larger than 1,000 nm. From the brightness of the plume, the total mass of particles was inferred to be between 10^8 and 10^{11} kg, with the larger values corresponding to smaller (1-nm) particles. Assuming a dynamical lifetime (flight

time) of order 10^3 seconds, these masses imply dust production rates of 10^5–10^8 kg s^{-1}.

On the other hand, Spencer *et al.* (1997) fit a Mie scattering law to color observations of Pele's plume taken by the Hubble Space Telescope (HST). Mie theory assumes that the particles are comparable in size to the light wavelength. Pele's scattering properties were fit by particles 50–80 nm in radius with a total dust mass of only 10^6 kg. Applying the same theory to the data of Collins (1981), the authors found that Loki's plume could also be accounted for by larger particles of 50 nm radius with a smaller plume mass of 10^6 kg, implying dust eruption rates of order 10^3 kg s^{-1}. Spencer *et al.* regarded their estimate as an upper limit, since the attenuation by Pele's plume could equally well be accounted for by SO_2 gas absorption in a vapor plume with a mass of 10^8 kg. Indeed, later HST observations (Spencer *et al.*, 2000) showed that much of the plume's opacity could be ascribed to gaseous S_2, further reducing the possible attenuation due to dust particles. The HST observations also suggested that Pele's plume is highly variable, appearing and disappearing on timescales of just 21 hours (Spencer *et al.*, 1997).

Geissler and McMillan (2006) fit Mie scattering models to *Galileo* visible color observations of the optically thick dust columns from Prometheus-type plumes. The results agree with those of Spencer *et al.* (1997), suggesting that the conspicuous dust plumes are made up of coarse-grained "ash" particles with radii on the order of 100 nm, and total masses on the order of 10^6 kg per plume. However, long-exposure images of Thor in sunlight show a faint outer envelope in addition to the optically thick core, similar to the structure of Loki. The outer envelope is apparently populated by particles small enough to be carried along with the gas flow, perhaps formed by condensation of sulfurous "snowflakes" as suggested by the plasma instrumentation aboard *Galileo* as it flew through Thor's plume (Frank and Paterson, 2002). The total mass of these fine, nearly invisible particles may be much greater than that of the coarser ash, and could account for significant resurfacing.

8.2.2 Gas

Plumes are also prominent at night and during eclipses, when they display an ethereal glow produced by the stimulation of the gases by charged particles, similar to terrestrial aurorae (Figure 8.4). The plumes can be seen at visible wavelengths as distinct knots or bubbles within an assortment of auroral glows that are present even when no plumes are active, including limb glows and equatorial emissions that periodically shift locations with the changing orientation of Jupiter's magnetic field. Only plumes near the electrical poles of Io (the sub-Jovian and anti-Jovian points) are in a position to be stimulated by the currents connecting Io to Jupiter. Exceptionally large plumes in other locations, such as the eruption of Tvashtar in late 2000, can sometimes be seen in emission because of the high density of emitting molecules.

The eclipse images show that the gas issuing from small Prometheus-type plumes extends much farther from Io's surface than the dust component, reaching heights and breadths up to 5 times as large as dust columns seen in daylight. The gases vented by

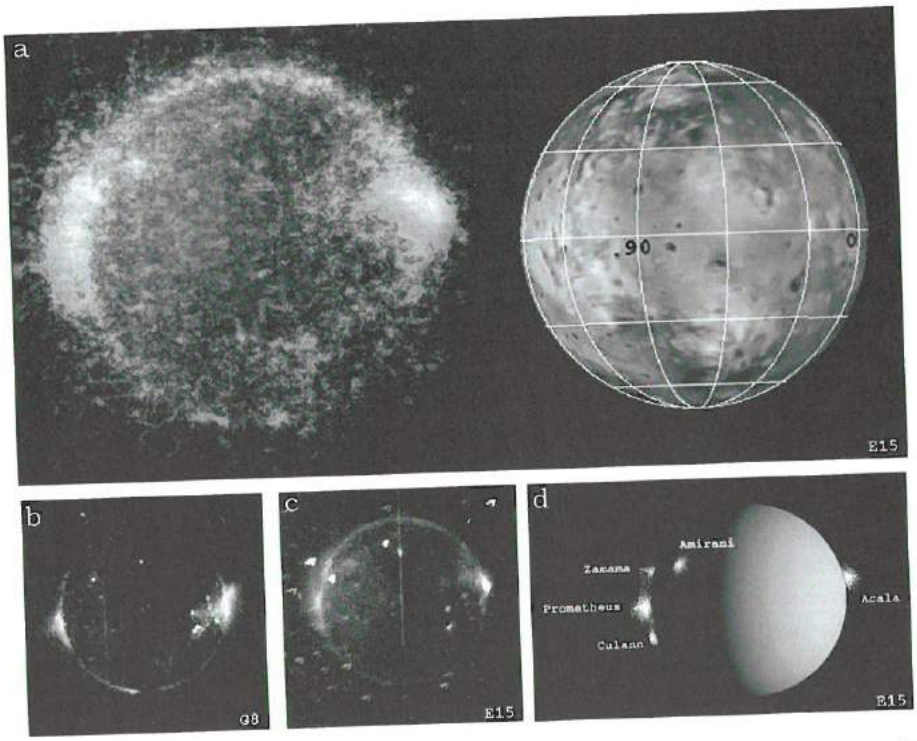

Figure 8.4. *Galileo* images of plumes in eclipse. (a) Visible-color image of atmospheric emissions during an eclipse in orbit 15 (*left*) compared with the sunlit appearance of the same hemisphere (*right*) (see also color section). The visible emissions are stimulated by charged particles, similar to terrestrial aurorae. The blue–white glows are produced by SO_2, and are concentrated at the locations of active plumes. The red and green glows are produced by atomic oxygen and atomic sodium, respectively (NASA press release image PIA01637). (b) Clear-filter image of the glows seen 1 year earlier, during the eclipse of orbit 8. The bright points on the disk show lava glowing by thermal emission. (c) Clear-filter image of glows seen during the eclipse of orbit 15. (d) Schematic diagram showing the locations of active plumes at the time of orbit 15 observations.

adjacent plumes often combine to form a megaplume above the most active regions. Some plumes such as Acala and Culann could be seen in emission during eclipse but were invisible in daylight, confirming a prediction (Johnson *et al.*, 1995) of the existence of stealth plumes that are largely free of dust.

The spectra of these auroral emissions yield information on the makeup and abundance of the gases, as well as the intensity of the electrical currents that excite the emissions (Geissler *et al.*, 1999, 2001a, 2004a). Molecular species such as SO_2 produce strong ultraviolet and visible continuum emissions that impart a bluish hue to the visible aurorae. The diffuse glows associated with the plumes in Figure 8.4 appear to be due to molecular SO_2 emission. Atomic species, including O, Na, and K, produce line emissions at longer visible and near-infrared wavelengths that are diagnostic of

their composition; however, present observations lack the spectral and spatial resolution needed to determine whether the abundance of atomic species in plumes differs from that of the background atmosphere.

Plume gases have also been identified spectroscopically at ultraviolet, infrared, and millimeter wavelengths. The observed gas compositions suggest two distinct classes of plumes. Sulfur-rich gases, including S_2, S, and SO, have been detected in Pele's plume along with larger abundances of SO_2 (e.g., McGrath *et al.*, 2000; Spencer *et al.*, 2000; Jessup *et al.*, 2004b). In contrast, only SO_2 was detected in spatially resolved ultraviolet observations of the Prometheus plume (Jessup *et al.*, 2004a), and the upper limit placed on the abundance of S_2 indicates a distinctly different composition for Prometheus than for Pele. However, temporal variations in the abundance of S_2 in Pele's plume were also noted (Jessup *et al.*, 2004b), including periods when it remained undetected. Recent microwave observations (Lellouch *et al.*, 2003) detected gaseous sodium chloride inferred to have been vented from volcanoes, providing a source for the Na and Cl detected in the atmosphere, neutral clouds, and plasma torus.

The observations of Jessup *et al.* (2004a) allowed them to estimate the excess column density of SO_2 gas at Prometheus at $5 \times 10^{16}\,\mathrm{cm}^{-2}$ and use this to derive a volcanic venting rate of $10^4\,\mathrm{kg\,s}^{-1}$. Slightly larger gas column densities were derived for Pele from earlier ultraviolet observations (Spencer *et al.*, 2000), but the larger volume of Pele requires an order of magnitude more massive plume.

8.3 OBSERVATIONS OF PLUME DEPOSITS

The deposits laid down by the plumes have also been studied with a variety of techniques. High-resolution images show the shapes, extents, and colors of the deposits, and the obvious changes in the appearance of the surface allow us to monitor plume activity over intervals between spacecraft visits. The thin SO_2 frosts deposited by many plumes are conspicuous at high phase angles, providing a means to identify sites of recent plume eruptions based on the optical scattering behavior of the surface (Geissler *et al.*, 2001b). Plume deposits can be clearly seen as fine grained frosts in the *Galileo* near-infrared mapping spectrometer (NIMS) measurements of the abundance and grain size of SO_2 as determined by infrared spectroscopy (Douté *et al.*, 2002).

Plume deposits can be annular, concentric, or irregular in plan. The sizes, shapes, and colors of the deposits divide into two categories, consistent with the two classes of plumes first suggested by *Voyager* observations of plume deposits (McEwen and Soderblom, 1983). Giant plumes produce enormous red rings up to 600 km in radius that are poor in SO_2 and may be dominantly made up of condensed sulfur. The smaller plumes produce SO_2-rich deposits that are typically less than 200 km in radius and are white or yellow in color unless contaminated with silicates. The two types of plume deposits are illustrated in Figure 8.5, which shows the superposition of the small plume deposit from Pillan on the giant red ring of Pele.

Pele's plume deposit consists of two parts: a black butterfly shaped pattern of ejecta near the patera surrounded by an enormous oval ring of red material. The dark

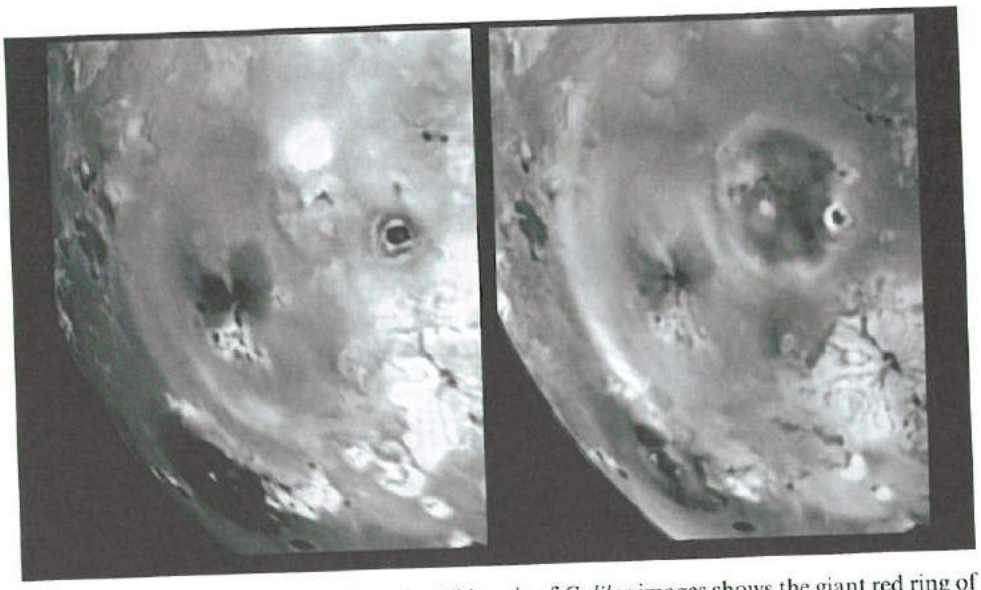

Figure 8.5. Two types of plume deposits. This pair of *Galileo* images shows the giant red ring of Pele, before (*left*) and after (*right*) the eruption of Pillan. Pele's annulus is elongated in the north–south direction, and reaches 720 km southwards from the source patera. Pillan's deposit is typical of small, SO_2-rich plumes that deposit ejecta up to 200 km from the eruption, except that it is colored by dark silicates (NASA press release image PIA00744). (See also color section.)

deposits changed very little during the period of *Galileo* observations, whereas the red ring was constantly in flux (Figure 8.1). These observations suggest two distinct populations of particles within Pele's plume. The composition of the dark inner deposits is not known, but it is reasonable to suspect that they may be made up of silicates entrained with the gas flow. Similar black deposits were emplaced by the nearby eruptions of Babbar and Pillan, and the near-infrared spectrum of these deposits shows an absorption feature at a wavelength of 0.9 μm, indicative of silicates (Geissler *et al.*, 2000). The red ring is elongated in the north–south direction, reaching a maximum radius of about 650 km. Several workers have suggested that Pele's red deposits are made up of short-chain sulfur allotropes such as S_3 and S_4 that are condensed from the gas phase (Moses and Nash, 1991; McEwen *et al.*, 1998; Spencer *et al.*, 2000; Moses *et al.*, 2002a). Faint bright deposits interior to the red ring appeared and disappeared during the *Galileo* observations, presumably caused by SO_2 entrained with or condensed by the plume.

Prometheus's deposit is a set of concentric rings superimposed on the older deposits laid down during the *Voyager* fly-bys (Figure 8.1). Color images taken during *Galileo*'s 8th and 14th orbits show four distinct rings, with radii of 72 km (bright yellow), 95 km (dark), 125 km (white), and 200 km (faint yellow, visible at high phase angles and prominent in NIMS SO_2 maps such as those in Douté *et al.*, 2002). In addition, the ghost of a ring fragment to the east is centered on the *Voyager* era plume

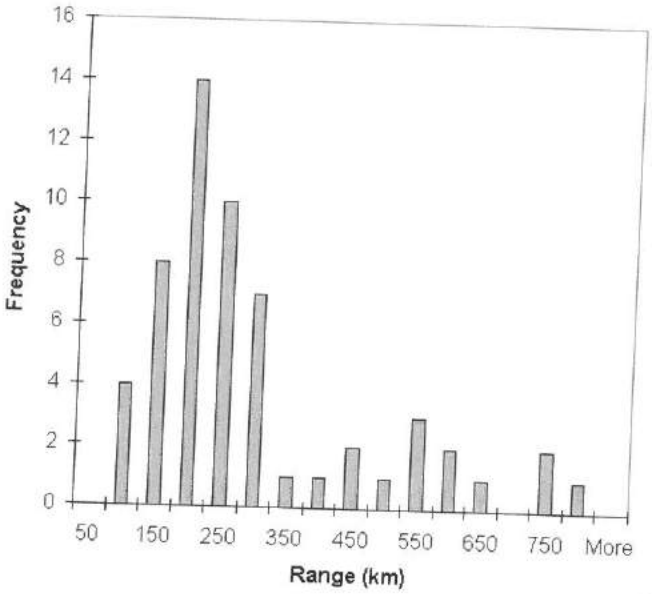

Figure 8.6. Maximum ranges of new plume deposits. This chart shows the frequency of plume-related surface changes observed on Io during the 5-year period of *Galileo* monitoring as a function of the maximum range of the deposits from their sources. The bimodal distribution results from the two distinct classes of plumes: the more numerous, smaller plumes produced deposits that reached no more than 300 km from their sources, whereas the giant plumes produced red rings with a broad range of radii averaging 600 km (from Geissler *et al.*, 2004b).

location. Concentric structures are common among rings and ring fragments from several other small plumes such as Culann, Zamama, and Marduk. An asymmetric red deposit stains the surface near Prometheus Patera, presumed to be the source of the silicate lava.

Many smaller explosive eruptions produce irregular deposits. Kanehekili's repeated eruptions seldom formed discernable rings. Irregular deposits alternated with circular structures at Amirani, Culann, Zamama, and Marduk. All of the red deposits flagging these eruptive centers are irregular; only giant plumes produce red rings.

Galileo's monitoring of Io over a 5-year period showed that surface changes took place repeatedly near the sites of many smaller plumes, indicating the sustained flow of lava from these volcanic centers. Pele's giant deposits also altered repeatedly throughout the mission, and ephemeral giant red rings appeared in several unexpected locations, including Tvashtar, Dazhbog, Surt and un-named volcanic centers south of Karei (12°S, 13°W) and near the north pole (80°N, 100°W). Some eruptive centers gave notice of impending explosions through changes in the brightness or color of patera surfaces prior to erupting. On the other hand, examples of episodic eruptions were seen from both classes of plumes that gave little warning beforehand and quickly returned to sleep afterward.

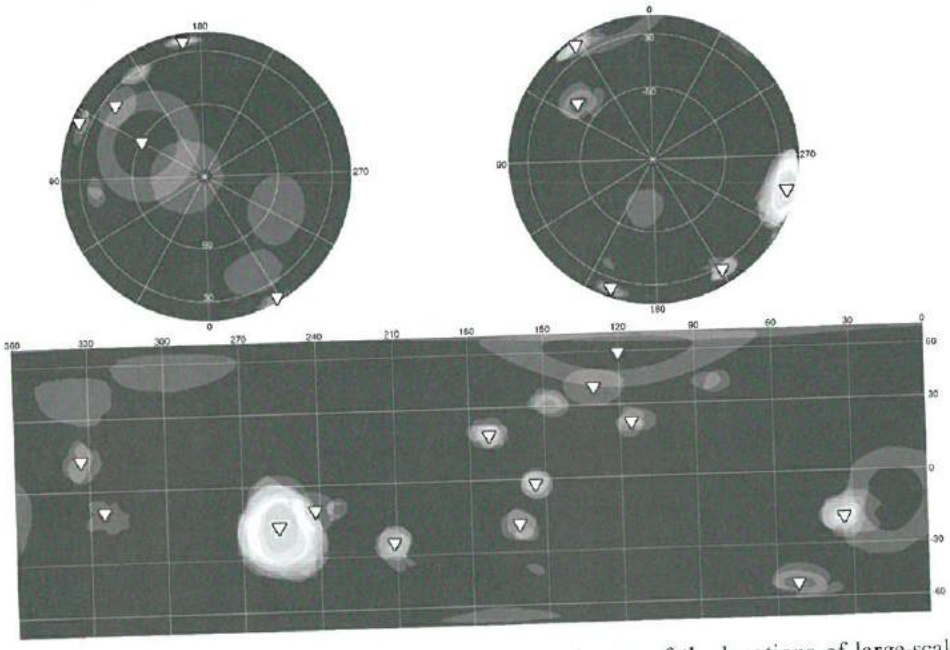

Figure 8.7. Plume deposits and plume sightings map. A map of the locations of large-scale surface changes (circular and irregular gray regions) and the sightings of plumes (triangles) during the *Galileo* era shows that every active plume produced visible changes in the appearance of the surrounding surface. In addition, several surface changes of similar character took place elsewhere on Io but the plumes that produced them were missed by *Galileo* (from Geissler *et al.*, 2004b).

The division between the two classes of plumes is clearly demonstrated by the bimodal distribution of maximum ranges of new plume deposits observed during the 5-year period of *Galileo* monitoring (Figure 8.6). All of the surface changes produced by the smaller, SO_2-rich plumes fell within 300 km of their sources, with most reaching only 200 km. All of the larger surface changes resulted from the emplacement of new red rings from giant plumes, with a broad range of sizes averaging 600 km in radius. A map of the locations of large-scale surface changes and the sightings of plumes on Io during the *Galileo* era (Figure 8.7) shows that every active plume produced visible changes in the appearance of the surrounding surface. In addition, several surface changes of similar character took place but the plumes that produced them were missed by *Galileo*.

8.4 PLUME SOURCES

The most thorough theoretical discussion of possible source reservoirs and vent geometries was presented by Kieffer (1982). She considered both SO_2 and S as potential driving fluids, and examined a variety of plausible initial conditions

ranging from low entropy (boiling liquids) to high entropy (vapors). She showed that flows emerging from depth through vertical conduits would be overpressurized relative to the ambient atmospheric pressure, but that expansion in a surface crater could reduce the pressure over relatively short distances (~1 km) to ambient. These would be pressure-balanced plumes, and would be likely to have a regular structure like the umbrella-shaped plumes. In contrast, flows erupting directly from conduits without such craters would be overpressurized relative to the ambient atmosphere, fluid velocities across the exit plane could vary wildly, and plume geometries would be expected to be irregular.

The plume sources so far observed on Io include lava lakes, lava flows, and fissures. No vents have been seen even in the highest resolution images, and craters that are several km across and more than 1 km deep can probably be ruled out by the observations. We suppose that the plumes are all overpressurized, and the difference between giant plumes and smaller plumes must result from the properties of the flow rather than the shapes of the vents.

Giant plumes appear to be produced by primary volcanic gases from paterae and lava lakes. Pele is a persistently bright hot spot at visible wavelengths, displaying temperatures (>1,500 K; Radebaugh *et al.*, 2004) consistent with freshly exposed mafic to ultramafic silicates (see Chapters 7 and 9). Close-up images of Pele at night (Figure 8.1) showed glowing lava near the margins of the patera, similar to actively overturning lava lakes on Earth. Fire-fountaining was seen at Tvashtar, driven by gases exsolved from the silicates. The fountaining lava reached more than a kilometer above the patera surface and was imaged by *Galileo* during orbit 25, just as Tvashtar began spouting its giant red ring. The red rings deposited by giant plumes are interpreted to be the condensation products of sulfur-rich gases that are absent from the smaller, SO_2-rich plumes. The dark diffuse deposits near the eruptive centers of giant plumes may be made up of silicate ash that was entrained with the flow, consistent with silicate sources. Given the high temperatures of the silicate magmas, the likely volatiles (S, SO_2) driving the giant plumes are certainly in the high entropy vapor state.

The smaller plumes all seem to be associated with lava flows. High-resolution images show the distinctive morphology of tube-fed flows of pahoehoe-type lava at Prometheus, Culann, Amirani, and elsewhere. Another crucial clue is the mobility of the plume sources. Loki developed a plume at a new location between the visits of *Voyager 1* and *Voyager 2*. Prometheus's source wandered more than 80 km westwards over the 20-year interval before the arrival of *Galileo*. Masubi's ring moved dramatically during the *Galileo* mission, and the centers of the disturbances at Amirani, Zamama, and Culann also shifted from one eruption to the next. In spite of these changes in location, the size and shape of Prometheus's plume appear remarkably constant over time. To account for this constancy, Kieffer *et al.* (2000) suggest that such plumes arise from shallow, choked conduits in the silicate lavas that allow subsurface slurries of molten SO_2 to vaporize and escape. They explain the steadiness of the eruption by noting that the mass eruption rate depends on the product of the subsurface fluid flow density times its velocity. In intermediate entropy fluids made up of mixtures of SO_2 liquid and vapor, the sonic velocity of the flow increases as the

density decreases, keeping the mass flux constant. Bright streaks of recondensed SO_2 can also be produced by small plumes at the margins of silicate lava flows (Milazzo *et al.*, 2001; Figure 8.1). Color images show venting of SO_2 from active jets near the flow front of Prometheus, as hot lava encroached on the frigid surface. The red deposits near Prometheus Patera and other eruptive centers are localized near the sources of the silicate lavas, consistent with the interpretation that the red materials are condensed from sulfur-rich gases directly exhaled by the silicates.

8.5 PLUME CHEMISTRY

The gases vented from the silicate magma provide important indications of the composition of Io's interior, along with the spectra of the lavas themselves. These gases originate in thermal equilibrium with the silicates but are subsequently altered by photolysis, condensation, chemical reaction, radiolysis, and recrystallization in equilibrium with the frigid surface ices or warm lavas upon which they fall.

Theoretical calculations (Zolotov and Fegley, 1999, 2000) of major volcanic gas chemistry, constrained by the observed abundances of S_2, SO, and SO_2 in Pele's plume (Spencer *et al.*, 2000; McGrath *et al.*, 2000), have been used to determine the oxygen fugacity of Pele's silicate lava. The implied high oxygen fugacity indicates that Io is differentiated and the mantle is free of metallic iron. These equilibrium calculations also yield estimates of the temperature of the magma (1,440 K) and the vent pressure (10^{-5} bar) of the plume.

Lesser abundances of the elements Na, K, and Cl are expected from alkaline ultrabasic magmas (Fegley and Zolotov, 2000). The composition of the vent gases depends critically on the (Na + K)/Cl ratio, which is still poorly known. High ratios should produce chlorides plus metals (Na and K), whereas chlorides plus chlorine are predicted for values of the ratio less than unity. Salts, sulfides, and sulfates are the expected condensation products in either case, and sputtering of these surface deposits probably contributes to the alkali metals and chlorine in the neutral clouds and plasma torus. Postberg *et al.* (2006) made the surprising finding that the dust escaping Io detected up to 1 AU from Jupiter by the Cosmic Dust Analyzer of *Cassini* was mostly made up of NaCl rather than sulfur compunds. Either NaCl dominates the dust composition because it is more refractory than sulfur species, or the dust that escapes is mostly NaCl because it is more easily ionized than sulfur species.

Compounds such as S_2 and S_2O require active volcanic sources because they are rapidly destroyed by sunlight after injection into Io's atmosphere, producing S, SO, O, and O_2 instead (Moses *et al.*, 2002a). Likewise, oxides of the alkali metals are quickly depleted by photolysis in favor of K, Na, Cl, KCl, and NaCl (Moses *et al.*, 2002b).

Substances vented by the plumes continue to alter even after condensation and deposition on the surface. The bright red hues of the giant plume deposits fade to pale yellows as short-chain sulfur allotropes such as S_3 and S_4 equilibrate to the more stable cyclo-octal form of sulfur (S_8). This fading takes place rapidly along the equator (on a timescale of months; Geissler *et al.*, 2004) but is inhibited at the reddish poles, either

because of lower temperatures or an increased flux of charged particles at high latitudes (Johnson, 1997). Along the equator, the fine grained frosts of SO_2 laid down by the smaller plumes are converted over time to coarse grained ices with markedly different light scattering properties (Geissler *et al.*, 2001b), presumably by annealing and recrystalization.

8.6 PLUME DYNAMICS AND MODELING

8.6.1 When plumes form

What features characterize a plume that make it distinct from other gas releases such as evaporation from a small region? It seems likely that there is a range of plume sizes and that some small ones or those lacking visible particulates ("stealth" plumes of Johnson *et al.*, (1995)) or obvious rings have simply not yet been observed. Perhaps three parameters, source density, temperature, and size, are sufficient to determine whether a gas source is a real "plume". Zhang (2004) examined circular disk sources of sublimating gas and found that when no surrounding sublimating atmosphere is present (at night), a ratio of thermal-based scale height to vent size, $S = RT/gr$, determines whether a source has enough thermal clout to develop a canopy shock. Here, R is the SO_2 gas constant, T the source surface temperature, g the surface gravity, and r the source disk radius. If $S > 1$, the source gas rises and expands and cools before forming a distinct canopy shock. Otherwise, the gas simply expands away from the source without shocking. If a gas source is too weak compared with a surrounding sublimation atmosphere, the atmosphere will confine it. Zhang (2004) suggests that for a distinct plume to rise above and blanket the atmosphere (rather than the other way around) the plume shock height should be greater than the scale height of the atmosphere. Also, the plume vent pressure should exceed the surrounding atmosphere surface pressure.

8.6.2 Types of plume models

Plume dynamics modeling can be broadly classified by the dimensionality of the flow and the manner of fluid representation. The simplest models would represent the plume as hemispherical or cylindrical uniform regions of effluent having no other spatial structure. Models in 1-D have been developed to explore the photochemistry of such plumes (Moses *et al.*, 2002a) but strong assumptions must be made about expansion and diffusion processes in the flow (e.g., eddy diffusion, thermal diffusion, no shocks). A 2-D flow representation is generally needed to accommodate the most important competing effects of gas-dynamic expansion and gravity. Moreno *et al.* (1991) simulated an axisymmetric plume and examined its interaction with a sublimation atmosphere. The most extensive axisymmetric simulations have been those of Austin and Goldstein (1995, 1998) and Zhang *et al.* (2003a,b,c; 2004) in which a range of detailed physical phenomena were explored. A fully 3-D representation is needed to understand non-simple sources, plume–plume interactions (e.g.,

Figure 8.5), and plume interactions with the flowing sublimation atmosphere or plume interactions with the Jovian plasma torus. No fully 3-D gas dynamic simulations have been presented.

Various models from Stochastic–Ballistic (SB) in the free-molecular regime, to rarefied gas dynamics in the transitional regime, to computational fluid dynamics (CFD) in the continuum regime, have been developed. The SB model, that simply tracks a spray of non-interacting particles, can satisfactorily reproduce aspects of the plume shape and ring deposition of some plumes by careful manipulation of the initial conditions. However, the thermal motion of individual particles and their collisions are not taken into account in an SB model so that the resulting flow field does not reflect features such as shocks or the acceleration and cooling of the gas through expansions which should occur at certain locations. Emitted radiation thus cannot be well modeled and motions of the gas molecules and entrained solid or liquid particles are independent of each other. The SB model may be suitable for understanding the small inclined sprays produced along the margins of intrusive lava flows (Milazzo *et al.*, 2001) because the length scales are small and gravity does not force the flow to fall back on itself. Larger volcanic plumes, however, exhibit a wide range of physical phenomena that can only be accommodated if the gas flow is at least partially collisional. Continuum CFD models capture more of the physics of the flow: they can be used all the way from the below-ground source of the effluent out into the expanding plume core flow. Yet beyond the several-kilometer-high core flow region, the gas may still continue to expand. In the intermediate region between the near-vent core flow and a much higher canopy shock (and, of course, from near the exobase on out to infinity) the Navier–Stokes equations of fluid mechanics do not apply and a rarefied gas model must be used. In such low-density flow regions, the continuum assumption breaks down because the mean free path of molecules becomes comparable to the length scale of flow (or radiating) features. However, the continuum approach may produce qualitatively reasonable solutions and may be the only current practical means of modeling some physics such as turbulence.

The difficulties posed by the SB and CFD flow models are overcome by the direct simulation Monte Carlo (DSMC) approach (Bird, 1994) which has been applied to volcanic plume modeling and sublimation driven flows by the UT Austin group. In the DSMC approach, fluid molecules and entrained particulates are individually represented as they translate and undergo collisions with each other and with boundaries. In DSMC a tremendous amount of physical detail can be included and the flow can be accurately modeled from deep within the continuum regions to the vacuum of space. DSMC is only limited by the prohibitive computational cost of modeling dense flows in which applicable Knudsen numbers are less than 0 (10^{-4} to 10^{-5}); for such flows a hybrid CFD/DSMC solution is needed.

8.6.3 Model boundary conditions

Regardless of the modeling approach chosen, the choice of reasonable boundary conditions is crucial. Among the most important of those boundary conditions are the source gas pressure, velocity, temperature, constituents, solid and liquid fraction,

particle size distribution, and level of non-equilibrium. Kieffer *et al.* (2000) have suggested that the tendency of the gases to be choked in nozzle-like conduits is a reasonable constraint. Yet the nature of the solid and liquid particles coming out of the ground is poorly constrained as is the level of non-equilibrium. Here, non-equilibrium refers not only to local thermo-chemical non-equilibrium, but also to the level of velocity and thermal slip between the co-moving gas and particles, the radiative non-equilibrium between the gas, the particles, and the surrounding vent or ground surface (Zhang *et al.*, 2003c and Zhang, 2004), and the thermodynamic non-equilibrium among different molecular energy modes within the gas (rotational, vibrational, translational). Most modelers to date have assumed complete equilibrium single or two-phase flow from a circular or point-like vent. The next most important boundary condition is the nature of the gas–surface interaction surrounding the source. (Solid or liquid particles that fall to the ground most likely stick.) Ingersoll (1989) assumed a sticking coefficient α. Zhang *et al.* assume $\alpha = 1$ (all stick) for incoming "condensible" molecules like SO_2 onto SO_2 ice but also assume a flux of molecules out of the surface to match the temperature-dependent equilibrium vapor pressure. Sticking coefficients are a crude way to model a little-known process in that they sweep many dependencies under the rug. But for microscopically rough and cold engineering surfaces in non-clean environments, it is often found that $\alpha = 1$ is a good approximation.

8.6.4 Stochastic/ballistic results

Some of the earliest theoretical results were those of Cook *et al.* (1979) using a shock front model and a SB model. Strom *et al.* (1981) and later Strom and Schneider (1982), examined these models further and introduced a few corrections. In the SB model, the representative gas particles introduced at a disk-like or point-like source are assigned initial velocities and are subsequently tracked until they strike the surface. Such an approach can reproduce certain observed features such as a domed canopy plume shape, circular ring deposits, and some of the brightness structure of the smaller Prometheus-type plumes. Lellouch in his 1996 review paper used a ballistic model to simulate volcanic plumes and interpreted the millimeter wave data to obtain a column density near the plume center of $\sim 10^{18}\,\mathrm{cm}^{-2}$ and the average column density over the plume of $\sim 10^{16}\,\mathrm{cm}^{-2}$, which agree better with that derived by Strobel and Wolven (2001), Feldman *et al.* (2000), and McGrath *et al.* (2000). Glaze and Baloga (2000) used the SB approach to try to solve the inverse problem of, given the apparent areal distribution of fallout in the main Prometheus ring, what combination of particle energies and flow angles near the vent are required? They suggest that the flow truncated beyond 75° from the vertical and a 0.08 standard deviation of particle speeds can reasonably reproduce the ring shape and size. However, it appears that the parameters they choose to match do not tightly constrain the needed source parameters and that the lack of consideration of collisional gas dynamics may bias the resulting conclusions about the source conditions. Douté *et al.* (2002) use the Glaze and Baloga model to study the evolution of surface patterns as the source region of the Prometheus plume moved. Long-term effects of sublimation and the re-exposure of underlying materials complicate the picture. Modestly good fits to the east/west areal

frost distributions are found if the movement of the source is uniform over time but the north/south distributions are not well reproduced. The SB model cannot account for the secondary humps in frost distribution outside of the main ring; those humps are likely a collisional gas effect. The SB model is almost certainly suitable for studying the motions of the larger (>1 mm) pyroclastic particles as they disengage from the gas flow just above the source, but is probably less suitable for studying gas flow.

8.6.5 Analytic results

Kieffer's (1982) model accounted for compressible, multi-phase flow and argued that a roughly conical crater could develop due to the erosion by high-speed exiting flow. The flow would reach such speed by gas-dynamic acceleration past a sonic throat (a local geometrical constriction) near the end of a possibly long conduit. Kieffer *et al.* (2000) suggest that the fact that the source of the remarkably unchanged Prometheus plume has wandered many kilometers between *Voyager* and *Galileo* monitoring indicates that the vent is a rootless conduit through the lava flow rather than dispersed lateral jets at changing places along the margin; lava overflows pre-existing snowfields, superheating the vaporizing products and producing the surprisingly constant shaped plume via choked two-phase flow.

8.6.6 Computational fluid dynamics results

Moreno *et al.* (1991) developed 2-D axisymmetric numerical models based on the conservation equations of inviscid, compressible gas dynamics to simulate both sublimation and volcanic atmospheres. They were the first to simulate the re-entry shocks but, due to a lack of spatial resolution and a narrowly focused jet-like input, did not find a canopy shock. Moreno *et al.* were able to model deposition rings, compute regions where snow condensation may occur in a plume, relate plume dynamic time- and length scales to loss mechanisms of atmospheric species to the plasma torus, and explore the relative contributions of the volcanic and sublimation atmospheres on the day and night sides of Io. Though they obtain flows having features modestly consistent with observations and more recent DSMC simulations, they have extended an inviscid flow model well beyond its range of applicability.

8.6.7 Direct simulation Monte Carlo results

Perhaps the most complete and detailed models of the plumes are provided by the DSMC simulations of Zhang *et al.* (2003a,b,c; 2004) based on the earlier DSMC simulations of Austin and Goldstein (1995, 1998). The Zhang papers include hot band transition in the rotational radiation model, discrete line emission from the three SO_2 vibration modes, a spherical planet with variable gravity, fully or partially coupled gas/dust flows, and multiple gas species. They find that the general umbrella-shaped plumes can best be created with nearly uniform vertical flow out of a circular source suggestive of a hot lava lake or a modestly deep conduit in which turbulent flow has made the velocity/density profile fairly uniform. A surrounding re-entry shock occurs

as the high Mach number expanding gas falls back on top of the ambient atmosphere. For this re-entry shock to occur, the stagnation pressure of the falling gas must be equaled or exceeded by the vapor pressure of the ambient atmosphere. The re-entry shock is oblique and as the gas subsequently expands, rises, and falls again it may undergo repeated bounces or re-entry shocks. Surprisingly, the flow through the re-entry shock can lead to either frost deposition or removal in different areas depending on the surface temperature; the post-shock gas may push away the upper reaches of the sublimation atmosphere thus reducing the surface pressure and creating radially outward winds that promote greater sublimation than condensation. Diurnally averaged frost deposition profiles, however, produce a net ring about where condensation occurs over the cold night-time surface.

By modeling small non-condensible particles in the flow, Zhang *et al.* (2004) are able to match several key observable features including limb photographs, photographs of the shadow cast by Prometheus, and ring structure. Figure 8.8 (from Zhang *et al.*, 2004) shows an attempt to match the *Voyager* limb image of Prometheus with entrained 1-nm particles. The gas column density shows a clear region of strong expansion and a canopy shock at about 50 km altitude. The surface temperature T_s on the left- and right-hand sides of Figures 8.8(b) and 8.8(c) are different and were chosen so that the dust column density images best match the *Voyager* data. This required a slightly greater T_s on the left (108 K) than on the right (106 K) to promote a slightly greater gas-dynamic bounce on the left. Particles tend to produce rings having sharp boundaries with a notable spike in deposition near the inner or outer ring edges, depending on the plume size. While particles larger than about 10 nm tend to deposit as the gas turns through the first re-entry shock, smaller particles turn with the gas and are deposited in an outer more broad ring. Other possible effluents move with the dominant SO_2 flow implying the following. (1) Even large fractions of S_2 (up to 40%) in the plume have a negligible influence on the plume structure because the gas cooling near the vent is dominated by expansion and vibrational line emission (radiation losses) from SO_2. (2) The primary deposition ring surrounding the vent is where virtually all vent material falls out (at $T_s < \sim 111$ K). There may be subsequent deposition rings but they consist mostly of material scoured off the surface below the primary re-entry shock. Since S_2 has a negligible vapor pressure at reasonable surface temperatures, it is not scoured and no subsequent S_2 rings are expected. Hence, Pele-type plumes have a single red ring. (3) Trace gas species entrained in the main SO_2 flow, such as sodium, are blocked by the SO_2 canopy shock from reaching appreciably above that shock. Hence, steady plumes even of Pele's scale do not appear capable of ejecting molecules or dust grains directly into escape trajectories without the intervention of some other source of energy (e.g., plasma heating of the plume canopies).

8.7 INTERACTIONS WITH THE ENVIRONMENT

The most obvious environmental effect of plumes is the rapid repainting of the surface with their colorful deposits. The eruption of Pillan blackened an area of $\sim 200{,}000\ \text{km}^2$

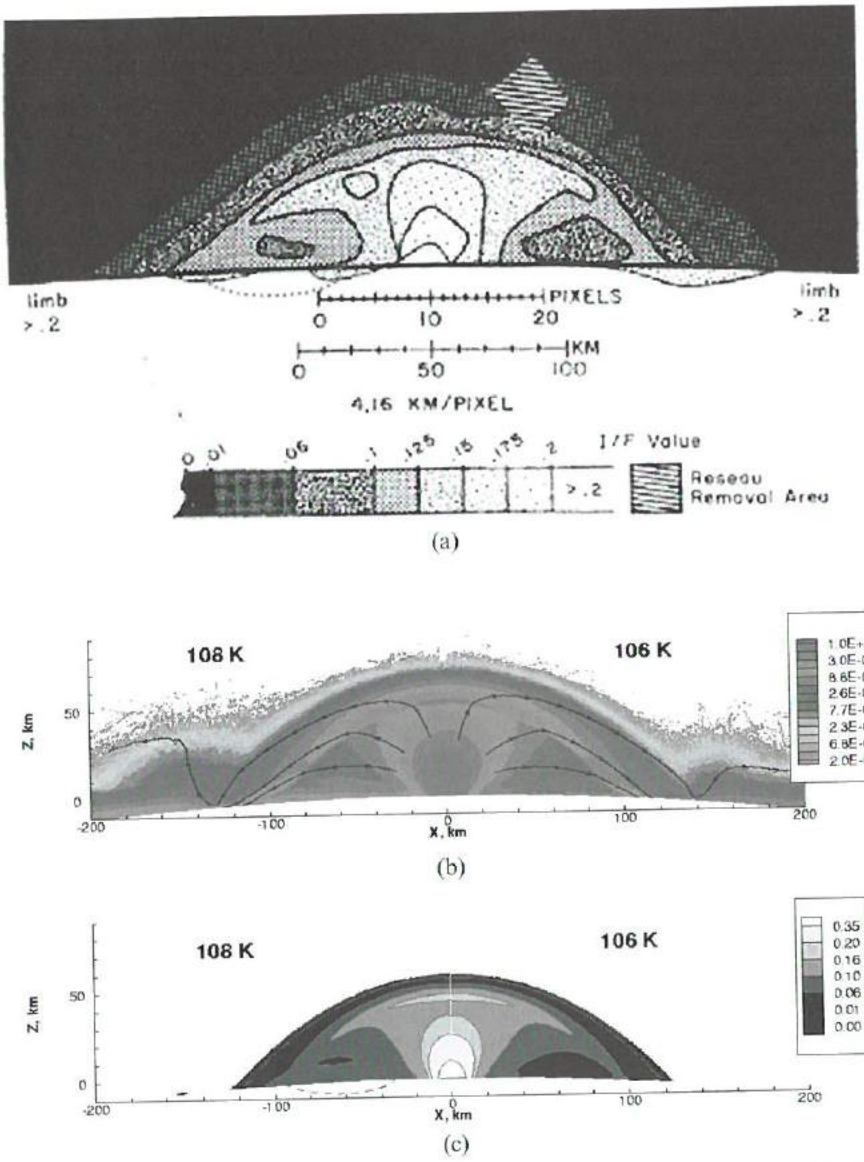

Figure 8.8. (a) *Voyager* image of the brightness of the Prometheus plume (from Strom and Schneider, 1982). Note the general sickle shape of the contours and the presence of a small signal near the surface on the left. (b) DSMC simulated number density contours (normalized by $5 \times 10^{16}\,m^{-3}$) of gas with a surface temperature of 108 K on the left and 106 K on the right. Select gas flow streamlines are also shown. (c) Normalized column density contours of 1-nm particles entrained in the gas flow. Notice the low altitude "dust cloud" circled on the left reflecting a settling time through the local atmosphere under the canopy of ~1,200 s. No cloud is seen on the right reflecting a settling time of only a couple of hundred seconds there. (See also color section.)

on a timescale of weeks, obscuring a large portion of Pele's red ring. Three years later, most of Pillan's pyroclastic deposits had vanished beneath a renewed red ring from Pele and bright frost from nearby Kaminari. Do the plume deposits simply coat the surrounding surfaces, or do they bury them? Estimates of the deposition rates of plume sediments vary greatly, ranging from 10^3 kg s^{-1} for Pele (Spencer *et al.*, 1997) to 10^7 kg s^{-1} for both Pele and Pillan (Cataldo *et al.*, 2002). A globally averaged resurfacing rate of ~1 mm yr^{-1} is required in order to account for the erasure of impact craters on Io (Spencer and Schneider, 1996), equivalent to the emplacement of 1,000 m^3 s^{-1}. Plume deposit thicknesses of order 5 mm yr^{-1} are needed to account for this resurfacing, given that roughly one-fifth of Io's surface was coated by plume fallout during the *Galileo* mission. Only massive plumes, with dust production rates of order 10^5 kg s^{-1}, could produce such deposition. Much of the resurfacing could instead be accomplished by the eruption of silicate lava flows: Amirani alone is estimated to have erupted 50–500 m^3 s^{-1} of new lava flows between subsequent *Galileo* observations, assuming that the flows were 1–10 m thick (Keszthelyi *et al.*, 2001). However, silicate lava flows cover only a small fraction of the surface, and the most powerful volcanic upheavals are confined to lava lakes like Loki. In contrast, plume deposits mantle areas that are hundreds to thousands of times greater than the lava flows and patera that produced them. This redistribution of material may account for the apparent absence of flooded and partially destroyed impact craters on Io.

There is no doubt about the significance of the contribution of volcanic plumes to Io's atmosphere. *Voyager 1* first identified SO_2 in Loki's plume that was attributed to volcanic outgassing (Pearl *et al.*, 1979). The earliest Earth-based detections of atmospheric SO_2 and SO showed spectral broadening and Doppler shifting that was ascribed to volcanic plumes (Lellouch *et al.*, 1990, 1992, 1996). As pointed out in Chapter 10, gases such as NaCl and S_2 that have negligible vapor pressure at Io's surface temperature require volcanic sources. The patchy nature of the tenuous atmosphere can best be explained by a combination of sublimation and volcanic venting (Ingersoll, 1989; Lellouch 1996; see also Chapter 10).

Once lofted into the atmosphere, the gas and dust ejected from plumes can be ionized by sunlight and impacting charged particles, swept away by the Jovian magnetic field, and spread throughout the Jovian system. Variations in the composition and mass of the neutral clouds and plasma torus are believed to be caused by volcanic eruptions on Io (Brown and Bouchez, 1997). Moses *et al.* (2002a) suggest that measurements of the S : O ratio in the plasma torus may be an effective means of remotely monitoring giant plume eruptions on Io. Correlations between the flux of ~10-nm dust particles recorded by the *Galileo* Dust Detector and the record of giant plume eruptions on Io during the 5-year tenure of the spacecraft indicate that ejection of dust from the most energetic plumes is chiefly responsible for the dust streams emanating from Io into interplanetary space (Krüger *et al.*, 2003).

The electrical currents that connect Io to Jupiter directly impinge on the plumes near the sub-Jupiter and anti-Jupiter points. Io is an effective electrical generator, powered by the magnetic field of Jupiter as it sweeps past the conducting satellite (Chapter 11). Part of Io's conductivity is through its ionosphere, but the conduction of

current into the interior of Io through plumes is an intriguing possibility (Gold, 1979). Spokes and filaments have been seen in Prometheus that appear similar to plasma-arc discharges observed in the laboratory (Peratt and Dessler, 1988), although they could instead result from multiple sources along the lava flow. Powerful currents could produce interesting disequilibrium chemical reactions within the plumes and possibly heat the surface of the satellite near the plume sources. These effects would be local, however, as the power generated globally by electrical induction is two orders of magnitude less than that derived from tidal heating.

8.8 CONCLUSIONS AND OUTSTANDING QUESTIONS

Recent observations and theoretical advances have filled many of the gaps in our knowledge of Io's plumes, but have also presented new puzzles. The process of assimilating the recent results and integrating the insights from different disciplines has not yet been completed, and we expect the list below will be expanded in the near future.

8.8.1 Conclusions

Several important lessons have been learned since the *Voyager* fly-bys and the subsequent analyses of those observations. The most obvious of these are summarized here.

- Extensive *Galileo* observations of dust plumes, gas plumes, and plume deposits confirm the post-*Voyager* suggestion (McEwen and Soderblom, 1983) that there are two distinct classes of plumes on Io. All of the plumes seen during the 5 years of *Galileo* observations can be described as either giant plumes, with characteristics similar to Pele, or smaller plumes that share the properties of Prometheus. Fundamentally, these two classes of plumes erupt from reservoirs at two distinct temperatures. Equating (to first order) the thermal energy of the plume gases to their kinetic energy and to the work done in transporting them across Io's surface, we have (Glaze and Baloga, 2000):

$$3/2\,kT = 1/2\,mv^2 = 1/2\,mgr$$

where r is the radius of a typical plume deposit, k is Boltzmann's constant, and the mass m is the same for both SO_2 and S_2. The observed factor of ~3 difference in ring radii for the two classes of plumes (~600 km for the giant plumes vs. ~200 km for Prometheus-types) implies a corresponding factor of ~3 difference in source gas temperature, assuming all other factors are equal.

- Both the gas and dust plumes were separately seen by *Galileo*, during eclipse and during day-time, respectively. In addition, *Galileo* eclipse observations confirmed the existence of high-entropy stealth plumes rich in gas but largely free of dust, as predicted by Johnson *et al.* (1995). More work remains to be done on these observations, particularly in cases where gas and dust plumes from the same locations were seen simultaneously or near-contemporaneously, but initial indications are that Prometheus-type gas plumes are larger than their dusty counterparts by a factor of 2–5. This mismatch in size suggests that the dust decouples from the gas flow in smaller plumes, and places a lower limit on the dust particle sizes, since dust smaller than ~10 nm is obliged to follow the gas for reasonably dense flows (Zhang *et al.*, 2004).
- The compositions of volcanic gases emitted from both Pele and Prometheus have been directly determined from HST ultraviolet observations. Sulfur-rich gases were detected in Pele's plume but not in that of Prometheus. This is consistent with the widely held interpretation (e.g., Spencer *et al.*, 2000; Moses *et al.*, 2002a) that Pele's brilliant red ring and other similar deposits elsewhere on Io are made up of short-chain sulfur allotropes such as S_3 and S_4 that are condensed from the gas phase. The composition of volcanic gases from Pele has also been used to infer the equilibrium chemistry of Io's interior.
- We have also determined that purely ballistic or hydrodynamic models are insufficient to describe the complexity of Io's plumes. Direct numerical simulations have revealed additional structures and phenomena that could not be recognized in earlier theoretical treatments, such as the patterns and strength of thermal emission, the distribution of particulates in the canopies, and the relationship between the background atmosphere, the surface temperature, and the deposition rings of condensates and particulates.

8.8.2 Outstanding questions

A number of new and old problems point out the weaknesses in our understanding of plume phenomena, and suggest directions for further research:

- Why are there two classes of plumes? The observed magma temperature of Pele (~1,500 K) and the temperature inferred from equilibrium chemical considerations (1,440 K) are equal to within the measurement uncertainty. The temperature of magma arising from deep sources is presumably controlled by tidal heating within Io and the mechanics of convection and eruption. By the arguments given above, the Prometheus-type plumes vent gases at ~1/3 of that temperature (i.e., 500 K or less), indicating a different energy source and/or driving fluid. Perhaps by coincidence, the critical temperatures of sulfur and of sulfur dioxide (above which they cannot be condensed) differ by a factor of 3.05. Sulfur's critical temperature is 1,313 K (Kieffer, 1982), little less than the probable temperature of silicate magmas erupting from Io's interior. We speculate that the maximum range of Prometheus-type plumes may be reached when encroaching silicate lava heats SO_2 to the critical temperature

(430 K for SO_2, Kieffer, 1982), at which point it can no longer be contained in the liquid phase.

- Where are the vents? The nature of plume vents or other source edifices is still unknown and poorly constrained by observations. While we have reasonably good simulations of rarified gas flow, the links to the subsurface source regions are presently lacking. Zhang *et al.* (2004) avoid this problem by postulating a virtual vent that is a circular source some distance above the surface with a fixed radius (order of kilometers), across which the initial conditions of the gas flow are assumed. Below this plane, the geometry of the source vent (be it the end of a long fissure or bubbles bursting in a lava lake) is undetermined.
- Does it snow on Io? The genesis of the dust in Io's plumes remains a mystery. There exists the possibility of snowfall on Io – condensation of S_x or SO_2 snowflakes or rain drops from the vapor phase as the plumes expand and cool – but the relative roles of condensation vs. lofting of existing dust particles are still unknown. It is theoretically possible, and appears observationally likely, that both entrainment and condensation take place in many of Io's plumes. At present, the particle sizes and implied mass eruption rates remain model dependent. The wider spectral range and better spectral resolution of the *Galileo* and *Cassini* imaging observations (in comparison with *Voyager* data) can be used to improve our knowledge of the dust particle size distributions and deposition rates.
- How do plume materials escape from Io? A reliable result of the numerical simulations is that steady, sufficiently dense plumes are effectively contained by their canopy shocks, preventing even very volatile species from directly escaping Io. On the other hand, volcanic influences on the population of ions in the plasma torus and on the flux of dust in the Jovian magnetosphere have been well established by the observations. One solution to this apparent contradiction could be unsteadiness in the vigor or supply of gas to the plumes. Pulses or other temporal variations in plume output invalidate the steady-state conditions assumed in the dynamical simulations and may provide the means for materials to penetrate the canopy shock and escape. Alternatively, addition of energy from solar or plasma heating may eject materials from the top of plumes, either directly (by imparting kinetic energy) or indirectly (by ionization, allowing external electrodynamic forces to sweep away gas and dust). Sputtering by charged particles may be the major means of atmospheric escape (Chapter 11).
- Other theoretical concerns. The implications of plume unsteadiness have yet to be investigated: if a plume pulses or suddenly shuts off, how long does it take before the effects are felt on the other side of Io? How long until the Jovian magnetosphere feels the change? Such knowledge is needed if we are to monitor plume activity on Io from, for example, changes in the S : O ratio of the plasma torus. In addition, the extent of the interaction between the plumes and the sublimation atmosphere remains an open issue. Properly addressing such questions presents a challenge for the future that will likely require a full 3-D, planet-wide simulation that includes both the dynamic atmosphere and the violent volcanic plumes of Io.

8.9 REFERENCES

Austin, J. V. and Goldstein, D. B. 1995. Direct numerical simulation of low density atmospheric flow on Io. In: M. Capitelli (ed.), *Molecular Physics and Hypersonic Flows*. Kluwer Academic Publishers, Dordrecht, The Netherlands, pp. 749–758.

Austin, J. V. and Goldstein, D. B. 1998. Simulation of Supersonic Rarefied Atmospheric Flows on Io. In: *Rarefied Gas Dynamics: Proceedings of the 21st International Symposium on Rarefied Gas Dynamics* (vol. 2). Cepadues-Editions, Toulouse, France, pp. 681–688.

Bird, G. A. 1994. *Molecular Gas Dynamics and the Direct Simulation of Gas Flows*. Oxford University Press, Oxford, UK.

Brown, M. E. and Bouchez, A. 1997. The Response of Jupiter's Magnetosphere to an outburst on Io. *Science*, **278**, 268–271.

Cataldo, E., Wilson, L., Lane, S., and Gilbert, J. 2002. A model for large-scale volcanic plumes on Io: Implications for eruption rates and interactions between magmas and near-surface volatiles. *Journal of Geophysical Research*, **107**(E11), 5109, doi:10.1029/2001JE001513.

Collins, S. A. 1981. Spatial color variations in the volcanic plume at Loki, on Io. *Journal of Geophysical Research*, **86**, 8621–8626.

Cook, A. F., Shoemaker, E. M., and Smith, B. A. 1979. Dynamics of volcanic plumes on Io. *Nature*, **280**, 743–746.

de Pater, I., Roe, H., Graham, J. R., Strobel, D. F., and Bernath, P. 2002. NOTE: Detection of the Forbidden SO a^1Delta$\rightarrow X^2$Sigma- Rovibronic Transition on Io at 1.7 mm. *Icarus*, **156**, 296–301.

Douté, S., Lopes, R., Kamp, L. W., Carlson, R., Schmitt, B., and The Galileo NIMS Team. 2002. Dynamics and evolution of SO_2 gas condensation around Prometheus-like volcanic plumes on Io as seen by the near infrared mapping spectrometer. *Icarus*, **158**, 460–482.

Fegley, B. and Zolotov, M. Y., 2000. Chemistry of sodium, potassium, and chlorine in volcanic gases on Io. *Icarus*, **148**, 193–210.

Feldman, P. D., Strobel, D. F., Moos, H. W., Retherford, K. D., Wolven, B. C., McGrath, M. A., Roesler, F. L., Woodward, R. C., Oliversen, R. J., and Ballester, G. E. 2000. Lyman-Alpha Imaging of the SO_2 distribution on Io. *Geophysical Research Letters*, **27**, 1787.

Frank, L. A. and Paterson, W. R. 2002. Plasmas observed with the Galileo spacecraft during its flyby over Io's northern polar region. *Journal of Geophysical Research (Space Physics)*, **107**, 31–1.

Geissler, P. E. and McMillan, M. 2006. Galileo observations of volcanic plumes on Io. *Icarus*, in review.

Geissler, P. E., McEwen, A. S., Ip, W., Belton, M. J. S., Johnson, T. V., Smyth, W. H., and Ingersoll, A. P. 1999. Galileo imaging of atmospheric emissions from Io. *Science*, **285**, 870–874.

Geissler, P. E., McEwen, A. S., Phillips, C., Keszthelyi, L., Turtle, E., Lopes-Gautier, M. M. R., Simonelli, D. P., Williams, D. A., and Galileo Imaging Team. 2000. New Results on Io's Color and Composition. *Lunar and Planetary Institute Conference*, Abstracts 31.

Geissler, P. E., Smyth, W. H., McEwen, A. S., Ip, W., Belton, M. J. S., Johnson, T. V., Ingersoll, A. P., Rages, K., Hubbard, W., and Dessler, A. J. 2001a. Morphology and time variability of Io's visible aurora. *Journal of Geophysical Research*, **106**, 26137–26146.

Geissler, P., McEwen, A., Phillips, C., Simonelli, D., Lopes, R. M. C., and Douté, S. 2001b. Galileo imaging of SO_2 frosts on Io. *Journal of Geophysical Research*, **106**, 33253–33266.

Geissler, P., McEwen, A., Porco, C., Strobel, D., Saur, J., Ajello, J., and West, R. 2004a. Cassini observations of Io's visible aurorae. *Icarus*, **172**, 127–140.

Geissler, P., McEwen, A., Phillips, C., Keszthelyi, L., and Spencer, J. 2004b. Surface changes on Io during the Galileo mission. *Icarus*, **169**, 29–64.

Glaze, L. and Baloga, S. 2000. Stochastic–ballistic eruption plumes on Io. *Journal of Geophysical Research*, **105**, 17579–17588.

Gold, T. 1979. Electrical origin of the outbursts on Io. *Science*, **206**, 1071–1073.

Ingersoll, A. P. 1989. Io meteorology: How atmospheric pressure is controlled locally by volcanos and surface frosts. *Icarus*, **81**, 298–313.

Jessup, K. L., Spencer, J. R., Ballester, G. E., Howell, R. R., Roesler, F., Vigel, M., and Yelle, R. 2004a. The atmospheric signature of Io's Prometheus plume and anti-Jovian hemisphere: Evidence for a sublimation atmosphere. *Icarus*, **169**, 197–215.

Jessup, K. L., Spencer, J., and Yelle, R. 2004b. Variability and Composition of Io's Pele Plume. AAS/Division for Planetary Sciences Meeting Abstracts 36.

Johnson, R. E. 1997. NOTE: Polar "Caps" on Ganymede and Io revisited. *Icarus*, **128**, 469–471.

Johnson, T. V. and Soderblom, L. A. 1982. Volcanic eruptions on Io: Implications for surface evolution and mass loss. In: D. Morrison (ed.), *Satellites of Jupiter*. University of Arizona Press, Tuscon, AZ, pp. 634–646.

Johnson, T. V., Matson, D. L., Blaney, D. L., Veeder, G. J., and Davies, A. 1995. Stealth plumes on Io. *Geophysical Research Letters*, **22**, 3293–3296.

Keszthelyi, L., McEwen, A. S., Phillips, C. B., Milazzo, M., Geissler, P., Turtle, E. P., Radebaugh, J., Williams, D. A., Simonelli, D. P., Breneman, H. H. *et al.*, 2001. Imaging of volcanic activity on Jupiter's moon Io by Galileo during the Galileo Europa Mission and the Galileo Millennium Mission. *Journal of Geophysical Research*, **106**, 33025–33052.

Kieffer, S. W. 1982. Dynamics and thermodynamics of volcanic eruptions: Implications for the plumes of Io. In: D. Morrison (ed), *Satellites of Jupiter*. University of Arizona Press, Tuscon, AZ, pp. 647–723.

Kieffer, S. W., Lopes-Gautier, R., McEwen, A., Smythe, W., Keszthelyi, L., and Carlson, R. 2000. Prometheus: Io's wandering plume. *Science*, **288**, 1204–1208.

Krüger, H., Geissler, P., Horányi, M., Graps, A. L., Kempf, S., Srama, R., Moragas-Klostermeyer, G., Moissl, R., Johnson, T. V., and Grün, E. 2003. Jovian dust streams: A monitor of Io's volcanic plume activity. *Geophysical Research Letters*, **30**(21), SSC 3-1, doi:10.1029/2003GL017827.

Lellouch, E. 1996. Io's atmosphere: Not yet understood. *Icarus*, **124**, 1–21.

Lellouch, E., Encrenaz, T., Belton, M., de Pater, I., and Gulkis, S. 1990. Io's atmosphere from microwave detection of SO_2. *Nature*, **346**, 639–641.

Lellouch, E., Belton, M., de Pater, I., Paubert, G., Gulkis, S., and Encrenaz, T. 1992. The structure, stability, and global distribution of Io's atmosphere. *Icarus*, **98**, 271–295.

Lellouch, E., Belton, M., Ballester, G. P., and de Pater, I. 1994. Millimeter-wave observations of Io's atmosphere: New data and new models. *Bull. Am. Astron. Soc.*, **26**, 1136.

Lellouch, E., Strobel, D. F., Belton, M. J. S., Summers, M. E., Paubert, G., and Moreno, R. 1996. Detection of Sulfur Monoxide in Io's Atmosphere. *Astrophysical Journal*, **459**, L107.

Lellouch, E., Paubert, G., Moses, J. I., Schneider, N. M., and Strobel, D. F. 2003. Volcanically emitted sodium chloride as a source for Io's neutral clouds and plasma torus. *Nature*, **421**, 45–47.

Lopes, R. M. C., Kamp, L. W., Smythe, W. D., Mouginis-Mark, P., Kargel, J., Radebaugh, J., Turtle, E. P., Perry, J., Williams, D. A., Carlson, R. W. *et al.* 2004. Lava lakes on Io: Observations of Io's volcanic activity from Galileo NIMS during the 2001 fly-bys. *Icarus*, **169**, 140–174.

McEwen, A. S. and Soderblom, L. 1983. Two classes of volcanic plumes on Io. *Icarus*, **58**, 197–226.

McEwen, A. S., Keszthelyi, L., Geissler, P., Simonelli, D. P., Carr, M. H., Johnson, T. V., Klaasen, K. P., Breneman, H. H., Jones, T. J., Kaufman, J. M. *et al.* 1998. Active Volcanism on Io as Seen by Galileo SSI. *Icarus*, **135**, 181–219.

McGrath, M. A., Belton, M. J. S., Spencer, J. R., and Sartoretti, P. 2000. Spatially resolved spectroscopy of Io's Pele plume and SO_2 atmosphere. *Icarus*, **146**, 476–493.

Milazzo, M. P., Keszthelyi, L. P., and McEwen, A. S. 2001. Observations and initial modeling of lava–SO_2 interactions at Prometheus, Io. *Journal of Geophysical Research*, **106**, 33121–33128.

Moreno, M. A., Schubert, G., Baumgardner, J., Kivelson, M. G., and Paige, D. A. 1991. Io's volcanic and sublimation atmospheres. *Icarus*, **93**, 63–81.

Moses, J. I. and Nash, D. B. 1991. Phase transformations and the spectral reflectance of solid sulfur: Can metastable sulfur allotropes exist on Io? *Icarus*, **89**, 277–304.

Moses, J. I., Zolotov, M. Y., and Fegley, B. 2002a. Photochemistry of a volcanically driven atmosphere on Io: Sulfur and oxygen species from a Pele-type eruption. *Icarus*, **156**, 76–106.

Moses, J. I., Zolotov, M. Y., and Fegley, B. 2002b. Alkali and chlorine photochemistry in a volcanically driven atmosphere on Io. *Icarus*, **156**, 107–135.

Pearl, J., Hanel, R., Kunde, V., Maguire, W., Fox, K., Gupta, S., Ponnamperuma, C., and Raulin, F. 1979. Identification of gaseous SO_2 and new upper limits for other gases on Io. *Nature*, **280**, 755–758.

Peratt, A. L. and Dessler, A. J. 1988. Filamentation of volcanic plumes on the Jovian satellite Io. *Astrophysics and Space Science*, **144**, 451–461.

Porco, C. C., West, R. A., McEwen, A., Del Genio, A. D., Ingersoll, A. P., Thomas, P., Squyres, S., Dones, L., Murray, C. D., Johnson, T. V. *et al.* 2003. Cassini imaging of Jupiter's atmosphere, satellites, and rings. *Science*, **299**, 1541–1547.

Postberg, F., Kempf, S., Sramaa, R., Green, S., Hillier, J., McBride, N., and Grün, E. 2006. Composition of jovian dust stream particles. *Icarus*, in press.

Radebaugh, J., Keszthelyi, L. P., McEwen, A. S., Turtle, E. P., Jaeger, W., and Milazzo, M. 2001. Paterae on Io: A new type of volcanic caldera? *Journal of Geophysical Research*, **106**, 33005–33020.

Radebaugh, J., McEwen, A. S., Milazzo, M. P., Keszthelyi, L. P., Davies, A. G., Turtle, E. P., and Dawson, D. D. 2004. Observations and temperatures of Io's Pele Patera from Cassini and Galileo spacecraft images. *Icarus*, **169**, 65–79.

Retherford, K. D., Moos, H. W., Strobel, D. F., Wolven, B. C., and Roesler, F. L. 2000. Io's equatorial spots: Morphology of neutral UV emissions. *Journal of Geophysical Research*, **105**, 27157–27166.

Roesler, F. L., Moos, H. W., Oliversen, R. J., Woodward, R. C., Retherford, K. D., Scherb, F., McGrath, M. A., Smyth, W. H., Feldman, P. D., and Strobel, D. F. 1999. Far-ultraviolet imaging spectroscopy of Io's atmosphere with HST/STIS. *Science*, **283**, 353.

Spencer, J. R. and Schneider, N. M. 1996. Io on the eve of the Galileo Mission. *Annual Review of Earth and Planetary Sciences*, **24**, 125–190.

Spencer, J. R., Jessup, K. L., McGrath, M. A., Ballester, G. E., and Yelle, R. 2000. Discovery of Gaseous S_2 in Io's Pele Plume. *Science*, **288**, 1208–1210.

Spencer, J. R., Sartoretti, P., Ballester, G. E., McEwen, A. S., Clarke, J. T., and McGrath, M. A. 1997. Pele plume (Io): Observations with the Hubble Space Telescope. *Geophysical Research Letters*, **24**, 2471–2474.

Strobel, D. F. and Wolven, B. C. 2001. The atmosphere of Io: Abundances and sources of sulfur dioxide and atomic hydrogen. *Astrophys. Space Sci.*, **277**, 271–287.

Strom, R. G., Schneider, N. M., Terrile, R. J., Cook, A. F., and Hansen, C. 1981. Volcanic eruptions on Io. *Journal of Geophysical Research*, **86**, 8593–8620.

Strom, R. G. and Schneider, N. M. 1982. Volcanic eruption plumes on Io. In: D. Morrison (ed.), *Satellites of Jupiter*. University of Arizona Press, Tuscon, AZ, pp. 598–633.

Zhang, J. 2004. Simulation of gas dynamics, radiation and particulates in volcanic plumes on Io. University of Texas at Austin PhD Dissertation, May, 2004.

Zhang, J., Goldstein, D. B., Varghese, P. L., Gimelshein, N. E., Gimelshein, S. F., and Levin, D. A. 2003a. Simulation of gas dynamics and radiation in volcanic plumes on Io. *Icarus*, **163**, 182–197.

Zhang, J., Goldstein, D. B., Varghese, P. L., Gimelshein, N. E., Gimelshein, S. F., Levin, D. A., and Trafton, L. M. 2003b. DSMC modeling of gas dynamics, radiation and particulates in Ionian volcanic jets. In: A. Ketsdever and E. P. Muntz (eds), *Proceedings of 23rd International Symposium on Rarefied Gas Dynamics* (vol. 663). AIP, New York, pp. 704–711.

Zhang, J., Miki, K., Goldstein, D. B., Varghese, P. L., and Trafton, L. M. 2003c. Modeling of radiation above Io's surface from Pele-type volcanic plumes and underground from the conduit wall. *Lunar and Planet. Sci.*, **XXXIV**, Abstract #2123.

Zhang, J., Goldstein, D. B., Varghese, P. L., Trafton, L. M., Miki, K., and Moore, C. 2004. Numerical modeling of ionian volcanic plumes with entrained particulates. *Icarus*, **172**, 479–502.

Zolotov, M. Y. and Fegley, B. 1999. Oxidation state of volcanic gases and the interior of Io. *Icarus*, **141**, 40–52.

Zolotov, M. Y. and Fegley, B. 2000. Eruption conditions of Pele volcano on Io inferred from chemistry of its volcanic plume. *Geophysical Research Letters*, **27**, 2789–2792.

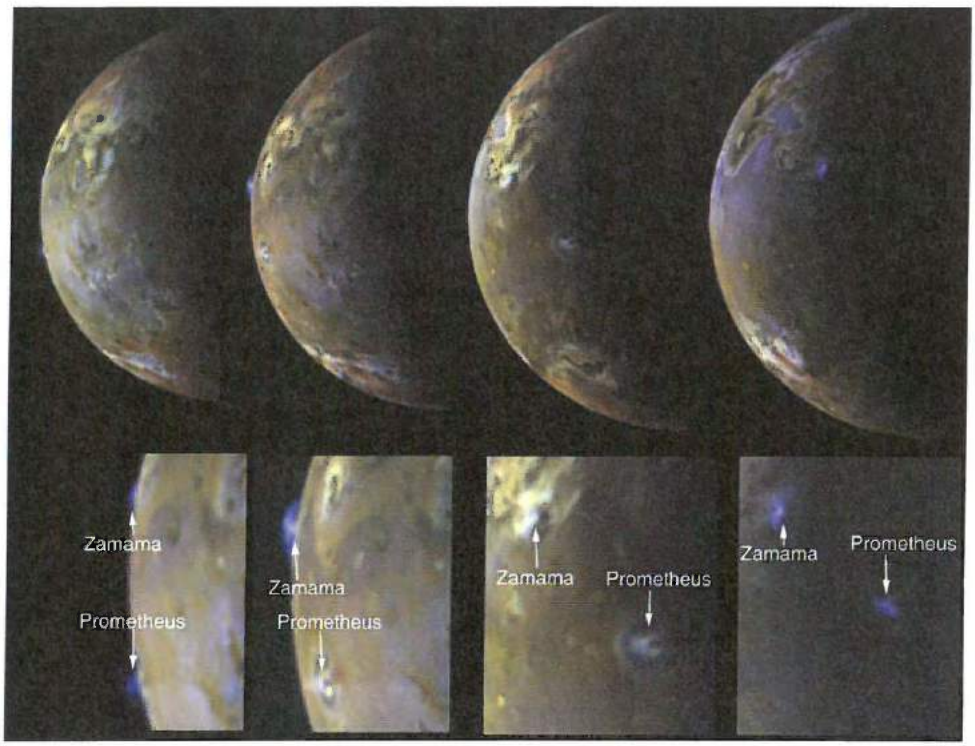

Figure 8.3. Zamama and Prometheus. This sequence of four images watches as two small plumes rotate onto the disk of Io. The blue colors of the plumes are caused by the light-scattering properties of the dust particles (NASA press release image PIA01652).

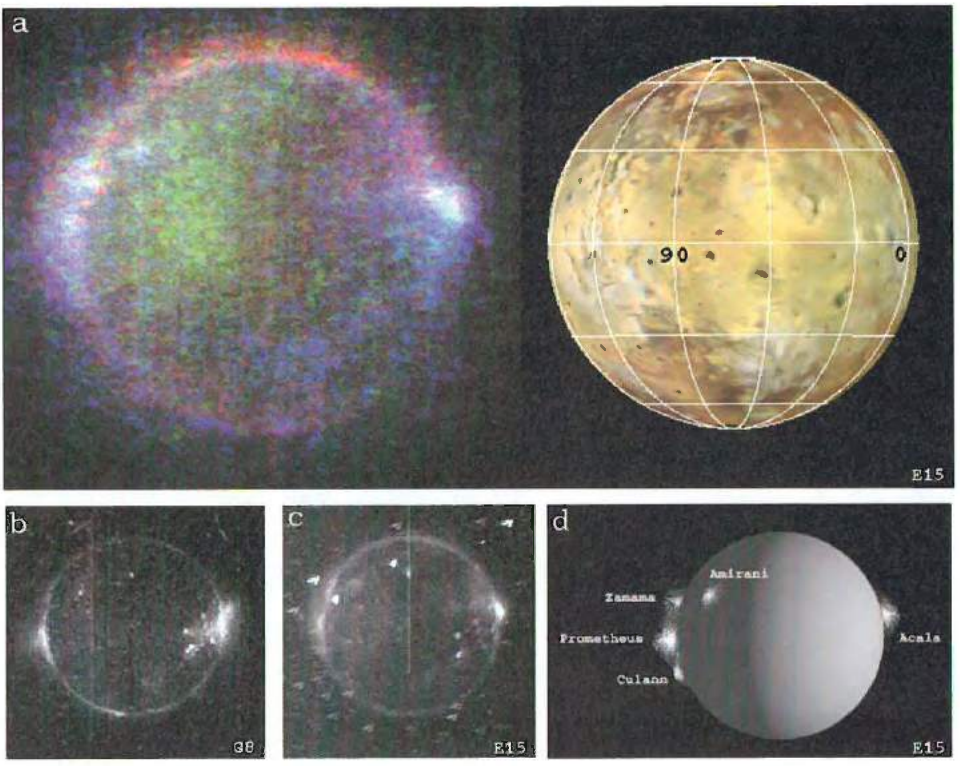

Figure 8.4. *Galileo* images of plumes in eclipse. (a) Visible-color image of atmospheric emissions during an eclipse in orbit 15 (*left*) compared with the sunlit appearance of the same hemisphere (*right*). The visible emissions are stimulated by charged particles, similar to terrestrial aurorae. The blue–white glows are produced by SO_2, and are concentrated at the locations of active plumes. The red and green glows are produced by atomic oxygen and atomic sodium, respectively (NASA press release image PIA01637). (b) Clear-filter image of the glows seen 1 year earlier, during the eclipse of orbit 8. The bright points on the disk show lava glowing by thermal emission. (c) Clear-filter image of glows seen during the eclipse of orbit 15. (d) Schematic diagram showing the locations of active plumes at the time of orbit 15 observations.

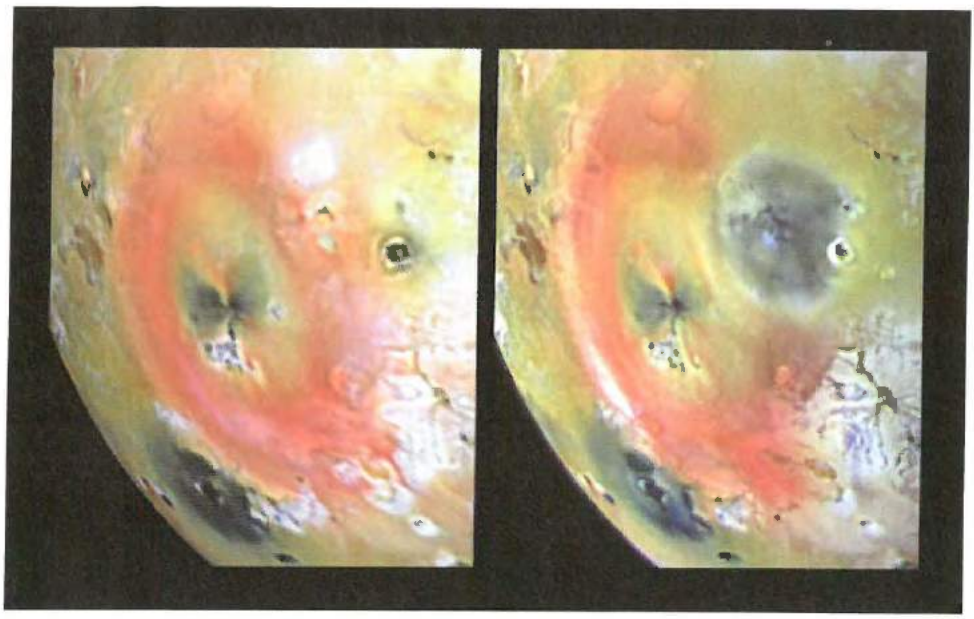

Figure 8.5. Two types of plume deposits. This pair of *Galileo* images shows the giant red ring of Pele, before (*left*) and after (*right*) the eruption of Pillan. Pele's annulus is elongated in the north–south direction, and reaches 720 km southwards from the source patera. Pillan's deposit is typical of small, SO_2-rich plumes that deposit ejecta up to 200 km from the eruption, except that it is colored by dark silicates (NASA press release image PIA00744).

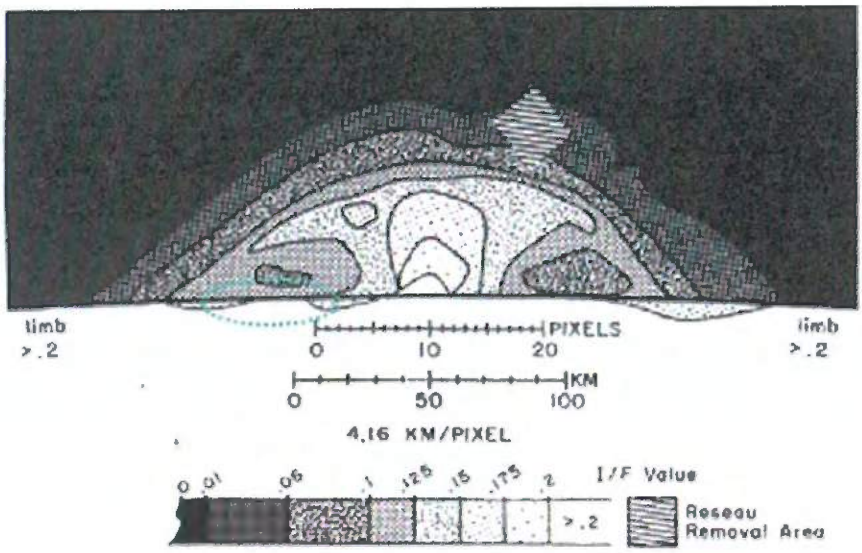

(a)

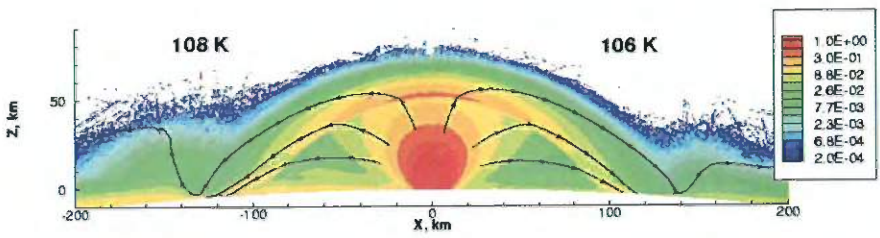

(b)

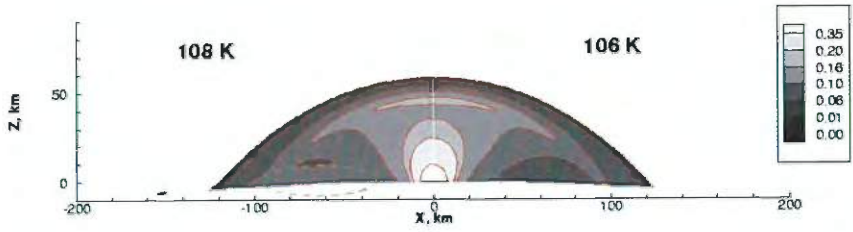

(c)

Figure 8.8. (a) *Voyager* image of the brightness of the Prometheus plume (from Strom and Schneider, 1982). Note the general sickle shape of the contours and the presence of a small signal near the surface on the left. (b) DSMC simulated number density contours (normalized by $5 \times 10^{16}\,\mathrm{m}^{-3}$) of gas with a surface temperature of 108 K on the left and 106 K on the right. Select gas flow streamlines are also shown. (c) Normalized column density contours of 1-nm particles entrained in the gas flow. Notice the low-altitude "dust cloud" circled on the left reflecting a settling time through the local atmosphere under the canopy of ~1,200 s. No cloud is seen on the right reflecting a settling time of only a couple of hundred seconds there.